PHILOSOPHICAL TRANSACTIONS OF THE ROYAL SOCIETY B BIOLOGICAL SCIENCES

Design of Graded-Index Lenses in the Superposition Eyes of Scarab Beetles

S. Caveney and P. McIntyre

Phil. Trans. R. Soc. Lond. B 1981 **294**, 589-632
doi: 10.1098/rstb.1981.0119

Phil. Trans. R. Soc. Lond. B **294**, 589–632 (1981) [589]
Printed in Great Britain

DESIGN OF GRADED-INDEX LENSES IN THE SUPERPOSITION EYES OF SCARAB BEETLES

By S. CAVENEY† and P. McINTYRE
Department of Neurobiology, Research School of Biological Sciences, Australian National University, Canberra, Australia 2600

(*Communicated by G. A. Horridge, F.R.S. – Received* 13 *February* 1981)

[Plates 1 and 2]

CONTENTS

† On leave from: Department of Zoology, University of Western Ontario, London, Ontario, Canada N6A 5B7.

Vol. 294. B 1075 42 [Published 23 September 1981

Superposition-image quality in the clear-zone eye depends in the first instance on the optical characteristics of the lens elements in each ommatidium. The optical design strategy of the two lens elements, a thick corneal facet and an underlying crystalline cone, in the scarab eye is reported. The formation of a good superposition image at the rhabdom layer in the eye demands that the lens elements be precisely arrayed, virtually free of optical aberrations, and that each lens pair function as an afocal (telescopic) lens system with an internal intermediate focal plane.

The optical properties of the corneal facet were examined by a variety of means. The isolated corneas of most scarab species focused good quality images of a distant object. Cardinal-point analysis of the intact corneal lens revealed that the back focal point of the lens lies just proximal to the inner corneal surface, many micrometres distal to the rhabdom layer, and the position of the principal planes suggested that the corneal lens had internal lens-cylinder properties. This was confirmed by the examination of the focusing power of transverse lens slices of known thickness; the power of the corneal lens slice was a function of its thickness. Interference refractometry of corneal sections revealed that the facet is a graded-refractive-index (g.r.i.) lens in the great majority of more than 40 scarab species examined. The position of the back focal point is achieved in a thick corneal lens by (i) the presence of a g.r.i. lens, best developed in the proximal corneal region, where it consists of a g.r.i. lens cylinder capped by a g.r.i. lens hemisphere, and (ii) the loss of front facet curvature in the homogeneous distal corneal region. *In situ*, the back focal point lies deep within the crystalline cone.

Since the quality of the superposition image depends on the exact location of the intermediate-image plane in the crystalline cone, this position was determined from a comparative analysis of cone shape, experimental observations, and theoretical modelling of the cone. Four observations, namely the presence of a waist in the crystalline cone of many species, the back focal distance of the isolated cornea when the refractive index (r.i.) of the medium in the back focal space approximated that *in situ*, the presence of screening pigment around specific regions of the crystalline cone and the position of the intermediate-image plane in the exocone of a passalid beetle eye, all suggested that the intermediate focus lies in the waist region.

The proximal region of the crystalline cone was modelled on the basis of its known g.r.i. lens properties. The model used comprised a radial g.r.i. lens cylinder with a parabolic profile in r.i., terminating in a g.r.i. lens hemiellipsoid. Dimensions and r.i. distribution in the model were based on values from real cones. The model cone focused an incident parallel beam to a point within the cone corresponding to the waist region in real cones. For beams at angles as great as 20° to the optic axis, aberrations in the model cone are small, and restricted to the most peripheral rays. A homogeneous hemiellipse of similar dimensions has severe aberrations for beams at an angle to the optic axis.

The model predicts that the ommatidial optics are diffraction-limited; the spread of rays leaving the proximal cone tip due to diffraction at the small exit aperture of the cone (for all aperture diameters) is broader than that due to lens aberrations. Consequently, tolerance exists to optical imperfections in the lens components and their spacing. A tolerance in the position of the intermediate focal plane of $\pm$ 2–3 μm was calculated.

Lens design is strongly correlated with the daily activity pattern of the scarab species under consideration. The corneal facets of nocturnal and crepuscular species are wide with little individual facet curvature; such 'glacial' corneas are completely transparent. The crystalline cone is large and well developed. In diurnal species, the corneal facets are narrower, with strong individual curvature, and the corneal lens cylinders are often lined with a brown screening pigment. The crystalline cones of diurnal scarabs are frequently strongly waisted or greatly reduced in size. Pigment surrounding the cone waist serves as a field stop limiting the angular acceptance of the ommatidial optics. The waist limits the number of ommatidia that can contribute to the superposition image and therefore determines the maximum aperture of the eye. This

PHILOSOPHICAL TRANSACTIONS OF THE ROYAL SOCIETY B BIOLOGICAL SCIENCES

aperture is greatest in nocturnal species with little or no waist constriction in the crystalline cone.

Most scarab clear-zone eyes are of the eucone type (separate crystalline cone). However, in the Passalidae and bolboceratine and pleocomine Geotrupidae, the crystalline cone is replaced by a corneal g.r.i. lens extension, the exocone, that serves as an optical analogue of the crystalline cone.

1. Introduction

Even at the turn of the century it was clear that the compound eye in the beetles (order Coleoptera) displayed extraordinary variety in the design of its dioptric elements and arrangement of photoreceptor cells (Kirchhoffer 1908). As early as 1891, Exner had classified insect eyes on the basis of function, into apposition eyes, characteristic of insect orders active during the day, and superposition eyes, generally found in insect orders whose members are predominantly crepuscular or nocturnal in activity. A necessary feature of a superposition eye is the presence of a wide 'clear-zone' (Horridge 1975) that separates the lens pair of each ommatidium, the corneal lens and the crystalline cone, from the photoreceptor layer of the eye.

In the typical diurnal apposition eye, the photoreceptor cells abut the crystalline cone and effectively receive light only from the lens system of the ommatidium in which they reside, because of the optical isolation of the ommatidia by screening pigment. Here the design strategy is to achieve a reasonable compromise between resolution and sensitivity in the compound eye. By contrast, the presence of a clear zone in the superposition eye allows parallel light entering the eye through many facets to cross between ommatidia and, in an ideal superposition eye, ultimately to focus upon the photoreceptor cells of the ommatidium whose optic axis is in line with the direction from which the light originated.† One way to achieve this is for the lenses of each ommatidium to form an afocal lens pair with an internal focus (intermediate image). Parallel light rays entering such a lens system leave it parallel (figure 1). Although the individual lens pairs are afocal, the radial array of the ommatidia in the compound eye allows a secondary image to be projected onto the receptor layer by the superposition of the beams emerging from the proximal tips of many lens pairs. The aperture of the superposition eye is set by the number of ommatidia contributing to a single image, whereas in the apposition eye the maximum aperture is limited by the diameter of a facet. According to Exner's theory, superposition improves the sensitivity of the eye, allowing it to function better at low light levels, without a significant loss in resolution. However, this requires that the lens elements be precisely aimed and largely aberration-free. That this accuracy can be achieved in superposition eyes is shown by the small angular distribution of eye shine in the day-active skipper butterflies and a day moth, *Phalaenoides tristifica* (Horridge *et al.* 1972; Horridge *et al.* 1977), but the superposition eyes of several other insects appear to be only poorly or 'partially' focused (Horridge 1975; Meyer-Rochow & Horridge 1975).

We felt that the question of superposition-image quality could not be resolved until the the optical properties of the ommatidial lens system were analysed in detail. Since many species of scarab beetles were available in Canberra we chose to investigate this group. The anatomy of the eye of scarabs (including the stag beetles, dung beetles and chafers) was first studied by Schultze (1868), Grenacher (1879), Bugnion & Popoff (1914), and in particular detail by

† For recent reviews on superposition optics in arthropod compound eyes, the reader is referred to Horridge (1975), Kunze (1979) and Land (1980*a*, *b*).

PHILOSOPHICAL TRANSACTIONS OF THE ROYAL SOCIETY B BIOLOGICAL SCIENCES

Kirchhoffer (1908). In the major scarabaeoid family, the Scarabaeidae (the true scarabs), the eye is of 'eucone' construction (Grenacher 1879), in which the refractile crystalline cone is separate and well developed. In each ommatidium the cone lies beneath a cylindrical corneal lens at the distal margin of a wide clear zone. Although the basic design of scarab compound eyes suggests that they are of the superposition type, most species previously examined are

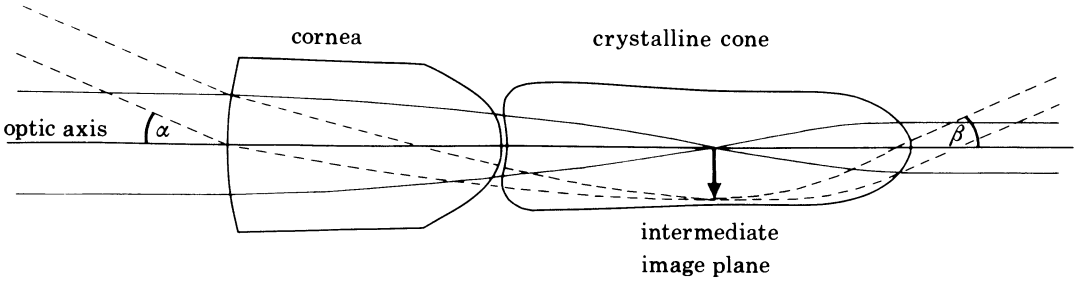

FIGURE 1. Ray paths through the lens system of a perfect superposition eye. Parallel light rays entering the optical system from the object space (left) are focused by the corneal lens and the distal crystalline cone to a point lying in the intermediate image plane. Pencils of light that enter the system at varying angles of incidence (α) to the optic axis are focused at different points in this image plane to create the primary, or intermediate, image. In the ideal state (the afocal or telescopic condition) parallel light rays entering the lens system leave it parallel. The ratio of the entrance angle α to the exit angle β is the angular magnification of the system. The function of the proximal tip of the crystalline cone is to project the intermediate image across the clear zone onto the photoreceptor layer of the eye.

day-active flower chafers and dung beetles, in which the cornea and crystalline cone appear to have undergone secondary modification probably associated with the reduced need for high sensitivity in bright light. Certain flower chafers even appear to have evolved an eye that functions as a clear-zone apposition eye (see the diagrams in Kirchhoffer 1908). On the premise that eye structure and function are primarily associated with flight navigation in scarabs, we felt that an accurate account of the optical properties of the dioptric systems of crepuscular or night-flying scarab species was long overdue.

Many workers have virtually ignored the role of the corneal lens in superposition eye function, concentrating instead on the (supposed) properties of the crystalline cone. We have taken a direct analytical approach in our study of both lens elements in isolation, and coupled our experimental findings to the optical theory of thick graded-refractive-index (g.r.i.) lenses (Marchand 1978).

The questions specifically asked were:

(i) *Is there a lens cylinder in the scarab cornea?*

The dioptric elements of the beetle eye appear to rely as much on the light-bending properties of their interiors as on refraction at exposed convex surfaces. In 1876, Exner reported that the corneal lens of the water beetle *Hydrophilus* appeared to possess the optical properties of a g.r.i. lens cylinder, an observation that he subsequently extended to the corneal lens process in the eye of *Lampyris* (Exner 1891). A g.r.i. lens cylinder is here defined as a cylinder of transparent material with a radially varying refractive index (r.i.) (Kapron 1970). In the beetle lens the highest r.i. is along the optic axis of the facet. Recently, Meyer-Rochow (1973) reported a g.r.i. lens cylinder in the cornea of the dytiscid beetle *Cybister*, but unaccountably failed to observe one in the anatomically similar eye of the scarab beetle *Anoplognathus* (Meyer-Rochow & Horridge 1975). Meyer-Rochow's conclusion was based, in part, on the interferometric

measurement of lens refractive index. We chose a more direct approach, namely to measure the focusing power of the isolated corneal lens and lens segments. This technique was first applied to the beetle eye by Exner in 1876, but has not been used since! Properly applied, it remains the simplest and most convincing demonstration of lens-cylinder properties.

(ii) *Where is the intermediate focus in the crystalline cone?*

Superposition theory demands that the dioptric elements in each facet of the eye form an afocal lens system in which the focal lengths are infinite, yet the two lens elements, the corneal facet and proximal crystalline cone, have finite focal lengths. The system becomes afocal when the back focal plane of the first element coincides with the front focal plane of the second element. A mismatch between these two focal planes results in light rays that have entered the system parallel diverging or converging on leaving the system. This would give rise to a poor or partially focused (Horridge 1975) superposition image. The ability to form a good superposition image is dependent on the position of the intermediate image within the crystalline cone. The position of this intermediate focus was analysed in several ways.

(iii) *What is the spread in the light emerging from the cone tip?*

The superposition image of a distant point source is a patch of light formed by the superposition of individual beams of light from each contributing ommatidium. The size of this patch is set by the spread in the individual beams and by the accuracy of alignment of the ommatidia to give a superposition of the beams. We are able to estimate the spread of individual beams from our analysis of the dioptric system.

(iv) *Why is the crystalline cone a graded-refractive-index lens?*

In the few instances where the r.i. profile of crystalline cones of nocturnal insects has been analysed by interference microscopy, the cones have been found to be strong g.r.i. lenses (Hausen 1973; Meyer-Rochow 1973; Meyer-Rochow & Horridge 1975). Although the overall shape of the scarab cone may vary considerably, the proximal tip is highly conserved, terminating in a rounded, typically hemiellipsoidal, g.r.i. lens. We have modelled the proximal end of the crystalline cone with appropriate values for its r.i. gradient and geometry, and compared its optical properties with those of a g.r.i. hemisphere and of an ellipse or sphere homogeneous in r.i.

(v) *Is lens design related to the daily activity pattern of a scarab?*

Most scarab groups, such as the leaf chafers (subfamily Rutelinae), the cockchafers (subfamily Melolonthinae), many dung beetles (subfamily Scarabaeinae) and the dorbeetles (family Geotrupidae), are primarily crepuscular or nocturnal in activity, but the flower chafers (subfamily Cetoniinae) are without exception day-flying species most active in bright sunshine. Many dung beetles, too, and certain stag beetles (subfamily Lampriminae) are strictly diurnal in activity. In several genera of dung beetle, related species may display extreme differences in patterns of daily activity. What adaptations in eye structure, particularly in the properties of the dioptric elements, are associated with diurnal activity in the scarabs? In comparing lens design in different species, attention was paid to the diel activity of the species concerned. This comparative approach was aided by recent studies on the diel activity rhythms of several dung beetle species that have been recently introduced into Australia as part of the Dung Beetle Project of the C.S.I.R.O. Division of Entomology.

PHILOSOPHICAL TRANSACTIONS OF THE ROYAL SOCIETY B BIOLOGICAL SCIENCES

2. Material and methods

(a) *Material*

Fresh beetles were used to obtain most of the optical data and interferometric measurements of refractive index given in this paper. Beetle corneal cuticle is remarkably stable, so that we were also able to use material fixed in 70% ethanol and even dried museum specimens in our comparative study of lamellicorn corneal structure. In the few instances where the focusing power of corneal lenses from fresh and alcohol-fixed sources (after rehydration in saline) was compared, little difference was noted. Our measurements of crystalline cone dimensions, too, are mainly based on fresh material, although alcohol preserves the cones well. The crystalline cones had shrivelled up in dried beetles.

In selecting beetle species for examination, our aim was twofold: to compare the general lens design in the eyes of as wide a selection of scarab families and subfamilies as possible, and then to concentrate on one subfamily (the scarabaeine dung beetles) for more subtle variations in lens anatomy. The beetles studied are listed below. The classification scheme adopted is that of Crowson (1955). Since a valid comparison of corneal structure in the different species (§4) cannot be made without reference to the physical size of the beetle concerned (corneal and general cuticle thickness in the mature adult is a function of body size) the body lengths of the specimens examined are also given:

Order Coleoptera: superfamily Scarabaeoidea (lamellicorn beetles)

			body length/mm
Passalidae	Aulacocyclinae	*Aulacocyclus edentulus* MacLeay	28
Lucanidae	Lampriminae	*Lamprima aurata* Latreille	22
	Lucaninae	*Lissotes rodwayi* Lea	12
		Cacostomus squamosus Newman	20
		Lucanus cervus L.	43
	Sinodendroninae	*Sinodendron cylindricum* L.	15
	Dorcinae	*Dorcus parallelopipedus* L.	26
Trogidae	Troginae	*Trox gigas* Harold	27
Geotrupidae	Geotrupinae	*Geotrupes spiniger* Marsh	24
		Thorectes chersimus Deladie	17
	Lethrinae	*Lethrus geminatus* Krtz.	23
	Frickinae	*Frickius variolosus* P.	18
	Bolboceratinae	*Blackbolbus frontalis* (Guér.)	24
		Stenaspidius albosetosus H.	8
	Athyreinae	*Neoathyreus excavatus* Group.	15
	Pleocominae	*Pleocoma behrensi* LeConte	23
Scarabaeidae	Melolonthinae	*Colpochila punctulata* Blanchard	24
	Rutelinae	*Anoplognathus* spp. 5 species of similar size (20–28 mm) and activity were used: *A. chloropyrus* Drapiez, *A. montanus* MacLeay, *A. pallidicollis* Blanchard, *A. porosus* (Dalman), *A. suturalis* Boisduval.	
		Repsimus manicatus Lea	17
		Phyllopertha horticola (L.)	10
	Dynastinae	*Dasygnathus trituberculatus* Blackburn	27
	Cetoniinae	*Cetonia aurata* L.	21
		Diaphonia dorsalis (Donovan)	27
		Oxytherea funesta (Poda)	10
	Aphodiinae	*Aphodius tasmaniae* Hope	10

PHILOSOPHICAL TRANSACTIONS OF THE ROYAL SOCIETY B BIOLOGICAL SCIENCES

Scarabaeinae–Onthophagini	*Phalops wittei* Harold	11
	Onthophagus gazella Heyd.	11
	O. taurus Schreber	10
	O. australis Guérin	9
	O. pentacanthus Harold	19
	O. mniszechi Harold	20
Scarabaeinae–Onitini	*Chironitis* (near *scabrosus* (Fab.))	14
	Onitis alexis Klug	19
	O. aygulus Latreille	25
	O. deceptor Péringuey	23
	Bubas bubaloides Janssens	20
	Megalonitis bohemani (Langsberge)	38
Scarabaeinae–Coprini	*Catharsius tricornutus* Degear	28
	Copris fallaciosus Gillet	23
	C. hispanus (L.)	23
	Heliocopris japetus Klug	50
Scarabaeinae–Scarabaeini	*Sisyphus spinipes* Péringuey	9
	Garetta nitens (Olivier)	17
	Scarabaeus sacer (L.)	35
	S. satyris Kolbe	29
	Kheper aegyptiorum (Latreille)	35
	K. prodigiosus (Erichson)	46
	K. nigroaeneus (Boheman)	30
	Pachylomera femoralis Kirby	45
	Pachysoma schinzi Fairmaire	30

(*b*) *Notation*

For convenience, a list of principal symbols and abbreviations used in this paper is given below.

F	front focal point
F′	back focal point
f	front focal length (focal length in object space)
f'	back focal length (focal length in image space)
g.r.i.	graded-refractive-index
H	first principal plane
H′	second principal plane
L	length of crystalline cone
λ	wavelength
M	angular magnification
n	refractive index
n_0	axial refractive index of lens cylinder
n_b	refractive index at lens boundary
Δn	$n_0 - n_b$
n_s	refractive index of medium surrounding cone tip
n_1	refractive index of medium in front focal (object) space
n_2	refractive index of medium in back focal (image) space
ϕ_d	diameter of corneal lens at distal margin
ϕ_p	diameter of corneal lens at proximal margin
ϕ_w	diameter of crystalline cone at waist
r	radius of lens cylinder
r_c	radius of curvature of outer corneal surface

r_d	radius of curvature of outer surface of individual corneal facets
r_p	radius of curvature of inner surface of corneal facet
r_1	radius of curvature of front surface of lens cylinder
r_2	radius of curvature of back surface of lens cylinder
r.i.	refractive index
s	distance between front surface of cornea and F (front focal distance)
s'	distance between back surface of cornea and F′ (back focal distance)
t	thickness of cornea along facet axis
θ_i	angle of incidence of ray at cone tip
θ_r	angle of refraction at cone tip
x	axial distance from centre of cone ellipse
x_a	intercept of ray on axis of cone
x_b	axial distance from centre of cone ellipse (or sphere) to boundary
x_i	value of x at point of ray incidence on cone boundary
y	radial distance from cylinder axis, or ellipse (or sphere) centre
y_b	radial distance from ellipse (or sphere) centre to cone boundary
y_i	value of y at point of ray incidence on cone boundary
y_b/x_b	ellipticity of crystalline cone tip

(*c*) *Optical analysis of isolated corneas*

A slice of cornea was cut from the eye with a razor blade, any adhering tissue carefully brushed away from behind it and the cornea floated on a drop of liquid of known r.i. (n) on a cover slip. The cover slip was placed on the stage of a compound microscope so that the illuminating light passed through the cornea either in the physiological direction (orthodromic illumination) or in the reverse direction (antidromic illumination). The microscope was used to examine the images formed by the corneal lenses of an object placed 50 mm away from the lenses (effectively infinity for the lenses, which have focal lengths of less than 100 μm). The medium on the outside of the cornea was air, that on the inside liquid, a good approximation to the *in vivo* situation when the r.i. of the liquid matched that of the crystalline cones in the eye.

The liquids used were a physiological saline ($n = 1.337$), solutions of bovine serum albumin in saline (Ross 1967) at various concentrations ($n = 1.38$–1.42) and immersion oil ($n = 1.515$). Vogt (1974) has shown that the first two liquids do not affect the r.i. of the cornea, and our own observations show that immersion oil does not alter the optical properties of the facet lenses at least over short periods of time. Initially glycerol was also tried, but it changes the intrinsic properties of the cornea, presumably by penetrating the cornea rapidly (as was also found by Vogt).

The optical parameters measured for each facet lens examined were the front and back focal lengths f, f' (see figure 2), the front and back focal distances s, s' (the distances between the front or back surface of the lens and the front or back focal points, respectively) and the thickness of the lens. From these measurements we determined the positions of the cardinal points H, H′ (the principal planes) and F, F′ (the focal planes) of the lens (figure 2). The significance of the cardinal points and the formation of images by lenses are covered in detail by most geometrical optics texts, for example, Longhurst (1973).

The focal distances were measured directly by focusing alternately on the surface of the lens and on the image formed by the lens, and reading the respective positions from a precision

micrometer gauge attached to the microscope stage. The difference between the two positions, corrected for apparent depth in the case of orthodromic illumination by multiplying by the refractive index of the liquid behind the cornea, in which the image was formed (Galbraith 1955; Blest & Land 1977), gives the appropriate focal distance, i.e. the back focal distance s' for orthodromic illumination and the front focal distance s for antidromic illumination.

The focal lengths were calculated from the image magnification; the size of the image of an

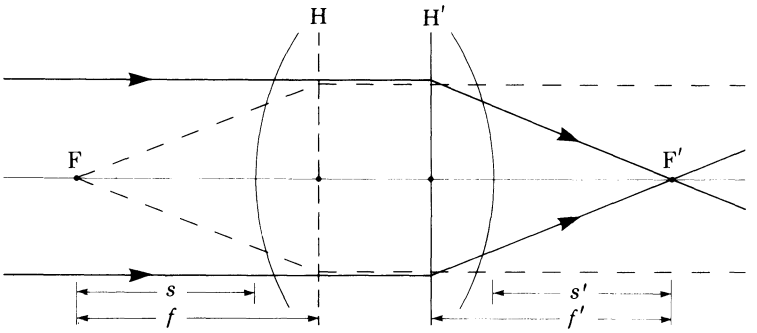

FIGURE 2. Cardinal points of a thick lens. A parallel beam of light entering a biconvex thick lens converges to form a real image of the source at focal point F′ in the back focal space. The distance between this back focal point and the pole of the back surface of the lens is the back focal distance s'. The back focal length f' is the distance between F′ and the back principal plane H′. F, H, s and f may be calculated by reversing the light path (dashed lines); s, s' measured from the respective lens surface, and f, f' from the respective principal plane, are positive if measured to the right, negative if measured to the left. Surfaces convex (concave) in the direction from which light is incident have a positive (negative) radius of curvature (convention after Longhurst 1973).

object of known size and (large) distance from the eye were measured with a calibrated eyepiece micrometer scale and the focal length calculated from (Blest & Land 1977):

$$\text{focal length} = \frac{\text{image size}}{\text{object size}} \times \text{object distance}.$$

This is an approximation, but is accurate when the object distance is large compared with the focal distance s or s' of the eye, a condition well satisfied in the present case. The front focal length f is measured with orthodromic illumination and back focal length f' with antidromic illumination, after correction for refraction at the liquid – cover slip – air interfaces (Blest & Land 1977).

The thickness of the lens was determined by cutting thin longitudinal sections through the appropriate region of the cornea and measuring with the eyepiece micrometer scale.

To determine the source of the refracting power of a lens, the candidates being refraction at the outer and inner surfaces and a r.i. gradient in all or part of the lens, the following parameters were also measured (figure 3): the radii of curvature of the inner and outer surfaces (by means of an eyepiece graticule with concentric circles of known radius), the diameter of the lens distally and proximally (tables 2, 3) and the r.i. or r.i. distribution of the lens.

(*d*) *Interference microscopy*

A Zeiss double-beam interference microscope was used to examine (at × 40 or × 100 objective magnification) sections of cornea or crystalline cone that had been cut with a hand-held razor blade (section thickness was typically between 10 and 20 μm). When a transparent object of uniform thickness is viewed in white light with interference optics, variations in r.i. within its

PHILOSOPHICAL TRANSACTIONS OF THE ROYAL SOCIETY B BIOLOGICAL SCIENCES

structure appear as differences in interference colour. An area of uniform r.i., or different regions of similar r.i., appear in the same colour (figures 8–13, plate 1). These colours are Newtonian interference colours, and consequently are not spectrally pure. If section thickness is constant, the sequence of interference colours (first order) yellow → mauve → (second order) blue → (second order) green indicates qualitatively a progressive increase in r.i. in the

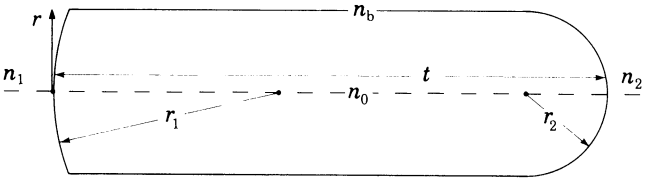

FIGURE 3. Parameters used in modelling the corneal g.r.i. lens. As a first approximation to the corneal lens cylinder, theoretical focal lengths and focal distances were calculated from a model of an axially uniform g.r.i. lens cylinder (thickness t and radius r) with two curved surfaces (radii of curvature r_1 and r_2). The axial and boundary r.i. (n_0 and n_b) and the r.i. profile were obtained from quantitative interference microscopy. This model fitted the experimental data for the lens well, even though the proximal corneal cap (c in figure 4) appears to function as a g.r.i. lens hemisphere. See §4*e*.

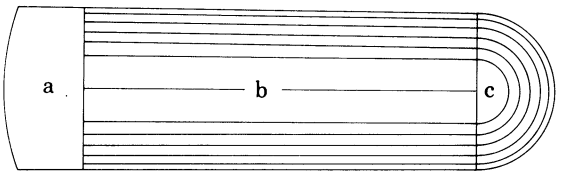

FIGURE 4. Components of the corneal g.r.i. lens. A scarab corneal facet has three optically distinct regions. The distal region of the corneal facet (region a) is uniform in r.i.; although its extent is variable, this isotropic region is usually less than 25% of the total corneal facet length (tables 2, 3). Region b is a g.r.i. lens cylinder. At its proximal margin it terminates in a g.r.i. lens hemisphere (region c).

region of the section examined. This method allowed instant identification of g.r.i. lens properties, as well as a determination of the extent to which the g.r.i. lens is developed in the cornea (regions b and c in figure 4).

For quantitative determinations of r.i., sections were examined in monochromatic light (λ = 546 nm) and values obtained by the extinction-point method of double immersion, as outlined in Ross (1967). The immersion fluids used were the saline and albumin solutions listed in §2*c*. The preparation to be examined was mounted on a Zeiss microrefractometer slide close to a well of known depth. An Ehringhaus rotary compensator was used to transfer the background extinction (black) to selected regions of the section. Readings were repeated several times for positive and negative angles of rotation of the compensator. These values were converted into differences in optical path length (retardation) and averaged. The r.i. of the immersion fluid was then obtained by extinction matching the content of the microrefractometer well to the glass of known r.i. around it, again by means of the compensator. This procedure was repeated by transferring the section into the second immersion medium, and extinction matching the same areas as used before. Double immersion allows the r.i. profile of the section to be calculated without knowledge of section thickness (Ross 1967). R.i. values obtained by this method have been rounded off to the second decimal place. These values are accurate enough for us to make valid predictions from the models in which they are used.

For rigid objects of cylindrical shape (for example, the intact crystalline cone) determination

of r.i. does not require double immersion, as the thickness of the object at any given point can be obtained geometrically from the cylinder dimensions. In this case, the crystalline cones were immersed in saline.

(*e*) *Theory of graded-refractive-index lenses*

The general theory of g.r.i. lenses is discussed in detail by, for example, Marchand (1978). The r.i. profiles used in the lens-cylinder models in this paper are of the form

$$n(r) = (n_0^2 - b^2 r^2)^{\frac{1}{2}},$$

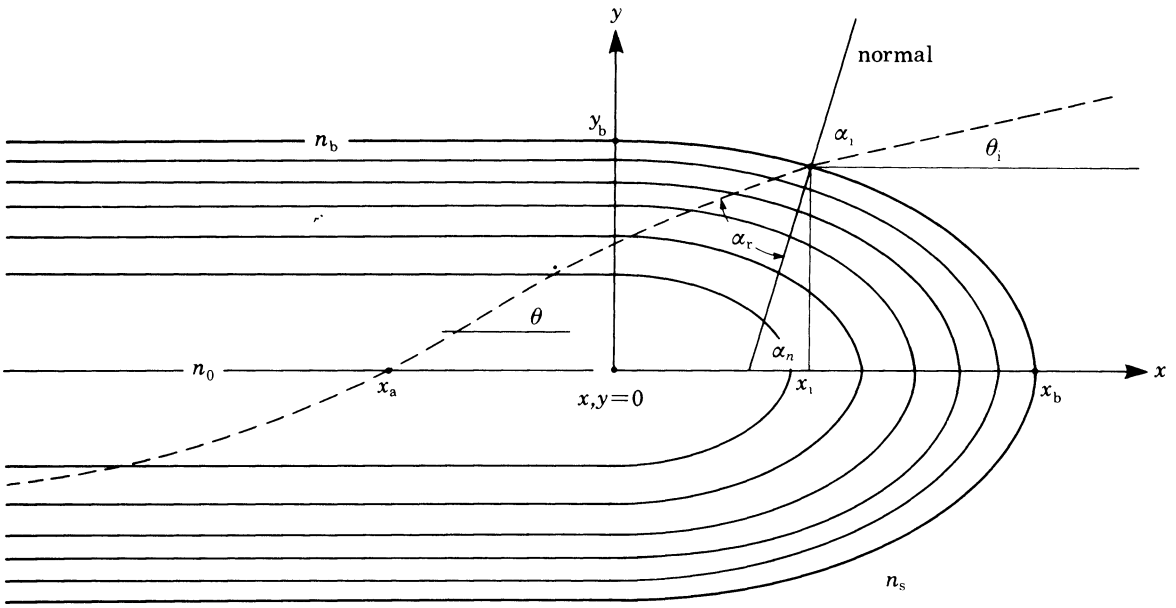

FIGURE 5. G.r.i. lens model for proximal ends of the corneal lens and the crystalline cone. α_r is the angle between the tangent to the ray immediately after refraction at the boundary and the normal through the point of intersection of the ray with the boundary; θ is the angle between the ray and the axis at any point x. The solid lines are contours of equal r.i. The other symbols are listed in §2*b*.

where n_0 is the r.i. on the axis of the lens and r is the distance from the axis. This is a good approximation to the profiles actually measured (see results) and, for the cases considered here, is very close to a parabolic profile. For this profile, analytic expressions for the ray paths (Meggitt & Meyer-Rochow 1975) and for the paraxial focal lengths and focal distances of a g.r.i. lens cylinder with two curved surfaces (figure 3; Sands 1971; Marchand 1978) can be found and the cardinal points located. Image quality for on- and off-axis rays can be determined by tracing rays through the lens. All ray calculations were carried out on an HP-97 programmable calculator.

In many cases the r.i. at the curved proximal tip of the corneal lens or crystalline cone does not vary with the square of the distance from the axis, but in an ellipsoidal or spherical manner, the surfaces of constant r.i. in this region being concentric with the back surface. The theory for this type of structure is presented below. By combining such a g.r.i. hemiellipsoid or hemisphere with a g.r.i. cylinder, a realistic model of both the corneal lens (figure 4) and the proximal part of the crystalline cone (figure 5) can be constructed. In all models we limit ourselves to meridional rays, i.e. rays passing through the optic axis of the lens. Only two-dimensional models need then be considered, the three-dimensional case (excluding skew rays) being generated by rotating the two-dimensional model about the optic (x) axis.

PHILOSOPHICAL TRANSACTIONS OF THE ROYAL SOCIETY B BIOLOGICAL SCIENCES

Consider the situation in figure 5. The refractive index at any point (x, y) in the elliptical part $(x \geqslant 0)$ is given by

$$n^2(x, y) = n_0^2 - a^2x^2 - b^2y^2, \tag{1}$$

where n_0 is the refractive index at the origin. The ray paths are given by the parametric equations (Luneburg 1964)

$$x = x_0 \sin(at + \phi_x), \tag{2}$$

$$y = y_0 \sin(bt + \phi_y), \tag{3}$$

where t is a parameter that increases along the ray path. This parameter t can be eliminated from equations (2) and (3) to give the equation for the ray path in the ellipse,

$$x = x_0 \sin\left\{\frac{a}{b}[\arcsin(y/y_0) - \phi_y] + \phi_x\right\}, \tag{4}$$

where x_0, y_0, ϕ_x, ϕ_y are found from the initial conditions x_i, y_i, θ_i:

$$x_0^2 = x_i^2 + \frac{n_b^2 \cos^2\theta_r}{a^2}, \tag{5}$$

$$\phi_x = \arctan\left(\frac{a\,x_i}{n_b \sin\theta_r}\right), \tag{6}$$

$$\phi_y = \arctan\left(\frac{b\,y_i}{n_b \sin\theta_r}\right), \tag{7}$$

$$y_0 = \frac{n_b}{b}\frac{\sin\theta_r}{\cos\phi_y}. \tag{8}$$

The angle θ_r, the angle that the ray makes with the x axis after refraction at the lens boundary, is found from Snell's law and the geometry of the ellipse (figure 5):

$$\theta_r = \alpha_n - \alpha_r, \tag{9}$$

$$\tan\alpha_n = b^2y_i/a^2x_i, \tag{10}$$

$$n_b \sin\alpha_r = n_s \sin\alpha_i \quad \text{(Snell's law)}, \tag{11}$$

$$\alpha_i = \alpha_n - \theta_i. \tag{12}$$

By means of these expressions and the corresponding ones for a lens cylinder (Meggitt & Meyer-Rochow 1975), rays can be traced through the lens (as in figure 25) to find the positions of best focus for different incident angles θ_i and to determine the quality of the image at these positions (effect of lens aberrations: see results). A spherical rather than ellipsoidal tip is obtained by putting $a = b$ in equation (1).

From the above expressions it can be shown that if the ratios of the r.i. $(n_0/n_b, n_s/n_b)$ remain constant, x_a and the focal lengths scale up in proportion to the linear dimensions x_b, y_b of the ellipse (figure 5). For example, if x_a is in the waist region of the crystalline cone, it will remain there as the dimensions of the cone are scaled up (y_b/x_b constant); a variation in cone size, as is found, will then have no effect provided that the intermediate image always lies at the cone waist.

An advantage of the model described above for the corneal lens and proximal crystalline cone is that it has general application (by appropriate choice of n_0, n_b, x_b and y_b) to any lens or cone with an ellipsoidal or rounded tip and a parabolic r.i. profile. (The model can in fact be

PHILOSOPHICAL TRANSACTIONS OF THE ROYAL SOCIETY B BIOLOGICAL SCIENCES

extended to other r.i. profiles with little difficulty.) We have used an analytic expression for the shape of the profile rather than the actual measured values because, to within experimental error, these values conform to the chosen profile, and by using the model we can easily determine the effect of different r.i. gradients on image quality and position. A profile of similar shape to the one used will give similar results because the ray paths are quite short. In this sense our choice of r.i. profile is not at all restrictive and allows us to explore the range of options available to the scarab eye in developing an effective optical system.

3. External appearance of the compound eye

The compound eye in most scarab beetles is partially or completely divided into a dorsal and ventral region by a horizontal cuticular process, the ocular canthus. The canthus intrudes into the front of the eye from the anterior margin. Consequently, although the surfaces of the dorsal and ventral regions of the eye may contribute to a common hemisphere, each region may form only a small segment of hemispherical eye surface. The ventral eye region is the larger of the two segments. Most scarabs have a partial canthus (Passalidae, ruteline and cetoniine Scarabaeidae). A few primitive species have no canthus at all (some Lucanidae), whereas in many advanced forms the canthus completely divides the eye externally (advanced Lucanidae and many dung beetles (Holloway 1969; Matthews 1972, 1974)). The canthus appears to have evolved to protect the eye during collisions in flight, and in the dung beetles, to shield the large ventral eye from abrasion during burrowing in soil and dung, when only the small dorsal region of the eye is exposed. In the dung-beetle genera *Scarabaeus* and *Geotrupes*, where a complete canthus is seen, the surface of the dorsal and ventral eye regions do not form segments of a common hemisphere, each having a curvature stronger than that of the eye as a whole. This, together with the fact that the ventral eye region is often more strongly facetted than the dorsal region (§4*b*), suggests that the two eye regions, particularly in the dung beetles, may serve different visual functions.

The field of view of the compound eye in beetles of similar morphology (e.g. the chafers) remains relatively constant over a wide range of increasing eye and body sizes (Buddenbrock 1952). Since the facet size remains relatively constant (diameter between 20 and 30 μm in most scarabs) it follows that facet number per eye may vary considerably. Buddenbrock states that the eye of the small June beetle *Phyllopertha horticola* has 3700 facets while the eye of the large chafer *Polyphylla fullo* contains 12150 facets. Here larger eyes have potentially greater resolving power, since more facets sample a given angle of the visual field. On the other hand, morphologically similar dung beetles of similar size may have eyes of quite different size and facet number (Matthews 1972, 1974); here eye size may be related to the greater diversity of activity patterns seen in the dung beetles (see §6*c*).

As the exoskeleton of the scarab is hard and typically very thick, it is not surprising that the corneal cuticle is also very solid. Unlike the general body cuticle, however, the cornea is highly transparent. A thick cornea immediately imposes constraints on corneal lens design that do not exist in insect eyes with thin corneas.

4. Design of the corneal lens

The structural diversity in the corneal facet of the compound eye in different scarab species suggests an astonishing range of design strategies. No standard design to the corneal lens is

evident. Instead, strong evolutionary pressure has fashioned this lens and the dioptric system as a whole to satisfy the optical requirements of differences in size, habitat and behaviour of member species. In diurnal species, the individual facets have a strong outer curvature absent in most nocturnal species. G.r.i. lenses are routinely seen in the thick corneas of large scarabs, although developed to varying extents. On the other hand, some small diurnal species have biconvex corneal lenses with uniform internal r.i. The inner surface of the corneal facet may

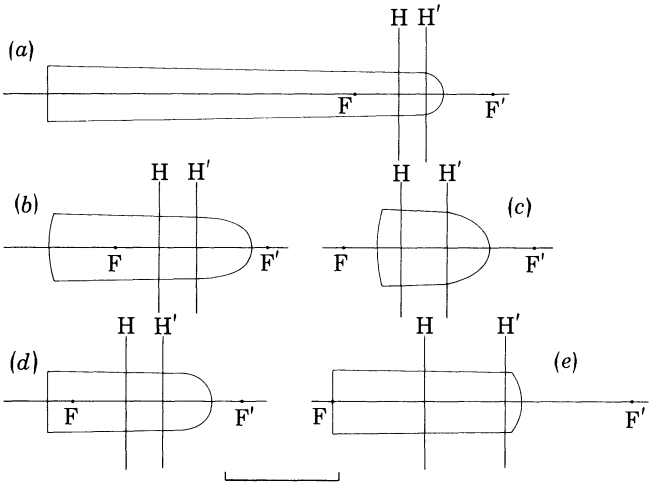

FIGURE 6. Cardinal-point analysis. The cardinal points of the isolated (but intact) corneal lens of five species listed in table 1 are shown. The corneal facets are all drawn to the same scale (scale bar, 50 μm). The front focal space (air, $n_1 = 1.000$) is on the left and the back focal space (saline, $n_2 = 1.337$) is on the right. The species shown are (*a*) *Lamprima aurata*, (*b*) *Geotrupes spiniger*, (*c*) *Onitis aygulus*, (*d*) *Anoplognathus* spp. and (*e*) *Copris fallaciosus*. The back focal point, F′ lies close to, but not within, the lens. The front focal point, F, may lie outside or within the lens.

Where the facet has a flat front surface (*a*, *d*, *e*) and the second principal plane, H′, lies within the lens, lens-cylinder properties may be inferred. The distance between H′ and the back surface of the lens is a measure of the extent to which the g.r.i. lens is developed along the lens axis in these cases. In *Anoplognathus* (*d*) it is well developed (see also figure 15) while in *Copris* (*e*) it is poorly developed (figure 11). In general, where the g.r.i. lens is well developed, the principal planes are located close to the centre of the lens cylinder (*b*, *c*, *d*).

have a short rounded projection, a *corneal cone* (typical of the majority of scarab species examined), or a long corneal extension, a *corneal exocone* (which we observed only in the passalids, bolboceratine geotrupids and *Pleocoma*). Brown pigment is found along the facet margins in many day-flying species, but is generally absent in crepuscular and nocturnal ones.

The aim of the next few sections is to show that, despite a wide range of structural modifications, the corneal facets of all species focus light to a point close behind the cornea (except species with exocones, where the focus is within the cornea). As we shall see, the position of this focus is critical to the overall functioning of the lens system, since it determines the ability of the eye to form a superposition image. The position of this back focal point was measured carefully for many species.

(*a*) *Cardinal-point analysis of the intact lens*

In the analysis of a thick lens or complex lens system it is often most convenient to consider the lens system in terms of its cardinal points (figure 2) without having to consider refraction at the series of surfaces within the system (Longhurst 1973). The location of the cardinal points of the lens may be found by the image magnification method (see methods). The thick beetle

cornea, being rigid and stable in a variety of immersion fluids, lends itself to this type of analysis. The cardinal points also allow a distinction to be made between homogeneous thick lenses and their non-homogeneous (g.r.i.) counterparts. In a homogeneous thick lens with a flat outer and a convex inner surface, the back focal point will be behind the lens and the back principal plane will form a tangent to the back surface. It is clearly not possible to obtain a back focal point inside this thick lens. On the other hand, a flat-front-surfaced g.r.i. lens with the same

TABLE 1. POSITION OF FRONT AND BACK FOCAL POINTS OF CORNEAL LENS

(The sign convention adopted here is described in figure 2; $n_1 = 1.000$; $n_2 = 1.337$.)

species	front focal length, f µm	front focal distance, s µm	back focal length, f' µm	back focal distance, s' µm
Lamprima aurata	−32	+140	+43	+22
Geotrupes spiniger (8)†	−37±2	+31±11	+49±1	+7±1
Anoplognathus spp. (8)†	−24±3	+11±4	+36±3	+14±1
Aphodius tasmaniae‡	−22	−10	+30	+17
Onthophagus pentacanthus‡	−48	−22	+66	+34
O. mniszechi	−38	+8	+47	+32
O. gazella	−28	−16	+38	+25
O. taurus	−21	−13	+33	+9
O. australis	−28	−6	+40	+14
Euoniticellus pallipes	−19	−13	+23	+10
Onitis aygulus	−26	−15	+40	+20
O. alexis	−27	−22	+47	+22
Bubas bubaloides‡	−37	−14	+52	+17
Catharsius tricornutus‡	−46	−18	+63	+50
Copris fallaciosus	−42	0	+57	+50
C. hispanus‡	−53	−1	+65	+58
Heliocopris japetus‡	−50	+155	+63	+60

† Number in parentheses refers to number of specimens studied. In these cases the mean±s.d. is given.
‡ Alcohol-fixed material. Other material was fresh.

external geometry can have its back principal plane deep inside the lens, and the back focal point may also lie inside the lens.

Irrespective of corneal thickness, the corneal lens in the scarab eye, with the exception of the exocone eyes, focuses incident parallel light to a point (F′) just behind the back surface of the cornea (figure 6). This focal point was readily measured, since the corneal facets of most species gave a sharp focus of distant objects (but see §4*g*). The point F′ often lies hundreds of micrometres distal to the photoreceptor layer in the eye. Measurements from the cleared corneas of many scarab species show that the back focal distance (distance of F′ behind the back surface of the cornea, s' in figure 2) is typically between 5 and 30 µm (although somewhat longer in coprine species), as listed in table 1, when the lens is floated in saline ($n = 1.337$). Furthermore, the back principal plane in corneas with flat front surfaces is many micrometres inside the lens (figure 6), i.e. the focusing power of these lenses is not solely due to refraction at the external surfaces, implying the presence of a g.r.i. lens. The location of the principal planes near, but not at, the proximal end of the corneal lens in most scarab species suggests that the power of the lens resides in this region (figure 6).

The primary role of the corneal lens is therefore to focus light to a point close to the back

surface of the lens. This focus is achieved in the thick cylindrical facet of the scarab cornea by one or a combination of three commonly seen design strategies:

(i) loss of or reduction in front facet curvature;

(ii) the presence of a g.r.i. lens cylinder, most strongly developed towards the proximal end of the corneal facet;

(iii) a g.r.i. lens hemisphere that caps the proximal end of the lens cylinder.

These three elements of the corneal lens are shown in figure 4; experimental and theoretical evidence for their presence is described below.

(*b*) *Loss of front facet curvature*

Giant scarabs, such as *Oryctes rhinoceros* (Bugnion & Popoff 1914) and *Heliocopris japetus* (figure 8), have a cornea that is at least six times thicker than the diameter of individual facets (tables

TABLE 2. CORNEAL LENS DIMENSIONS IN REPRESENTATIVE SPECIES OF FIVE SCARABAEOID FAMILIES

		cornea		individual facets					
FAMILY, subfamily, *species*	flight activity†	t µm	r_c µm	ϕ_d µm	ϕ_p µm	r_d µm	r_p µm	extent of g.r.i. lens (%)	reference‡
PASSALIDAE									
Aulacocyclus edentulus§ (4)	N	278	800–1000	41	35	r_c	exocone‖		1
LUCANIDAE									
Lamprima aurata§	D	180	650	25	19	r_c	−9	90	1
Lissotis rodwayi	F	95	520	26	20	r_c	−13	80	1
Cacostomus squamosus	N	105	550	32	26	160	−10	70	1
TROGIDAE									
Trox gigas	F	116	650	33	28	r_c	−13	75	1
GEOTRUPIDAE									
Geotrupes spiniger§ (7)	CN	93	840–1020	31	28	60	−13	>90	1
Blackbolbus frontalis	N	150	1250	25	23	r_c	exocone‖		1
Stenaspidius albosetosus	D	83	400	20	16	21	exocone‖		1
Pleocoma behrensi	?	148	980	33	31	r_c	exocone‖		1
SCARABAEIDAE									
Melolonthinae									
Colpochila punctulata	CN	88	940	26	24	r_c	−11	>75	1
Sericesthis geminata	CN	70	800	28		r_c	−13		2
Melolontha vulgaris	C	90		30					4
Rutelinae									
Anoplognathus spp.§ (8)	C	76	900–1100	28	26	r_c	−11	75	1
Phyllopertha horticola	D	50	160	23	21	31	−10	>90	1
Dynastinae									
Oryctes rhinoceros	N	172		25		r_c			3
Dasygnathus trituberculatus	N	122	990	28	24	r_c	−11	74	1
Cetoniinae									
Diaphonia dorsalis	D	111	660	27	24	100	−7	93	1
Aphodiinae									
Aphodius tasmaniae	C	43	320	25	22	r_c	−10	75	1

† D, day; C, crepuscular; N, nocturnal; F, flightless. In the absence of more precise data, many species are described in this table (and in tables 3 and 4) as night-flying on the basis of being attracted to lights at night.

‡ References: 1, present study; 2, Meyer-Rochow (1977); 3, Bugnion & Popoff (1914); 4, Grenacher (1879).

§ Fresh material. Where given, numbers in parentheses indicate specimens studied.

‖ In species with exocone corneas, the thickness value given is that for total cornea. The exocone dimensions for *Aulacocyclus* are given in table 4.

2, 3), as has the stag beetle *Lamprima aurata* (figure 6*a*). The cornea has a smooth and glassy outer surface in such species. The reason is simple. A strong front-surface curvature to the individual facets would result in the back focal point lying within the cornea. (If the scarab cornea were homogeneous in r.i., one can calculate that a front facet curvature of radius less than about half that of the overall corneal thickness would result in an internal focal point.) A smooth outer surface to the cornea, in which the radius of curvature, r_d, of the individual facets is equal to that of the corneal surface r_c (see tables 2, 3), is common in many crepuscular and nocturnal species.

Strong front curvatures to the individual facets are seen, however, in large chafers (Cetoniinae)

TABLE 3. CORNEAL DIMENSIONS IN DUNG BEETLES (SUBFAMILY SCARABAEINAE)†

tribe *species*	flight activity‡	t µm	r_c µm	ϕ_d µm	ϕ_p µm	r_d µm	r_p µm	extent of g.r.i. lens (%)	corneal screening pigment§
Onthophagini									
Phalops wittei	D	38	390	18	16	36	−11	>90	+++
Onthophagus gazella‖	C	44	450	26	25	120	−13	77	−
O. taurus‖	D	48	600	23	20	26	−10	>90	+++
O. australis‖	D	60	650	23	21	37	−10	>90	+++
O. pentacanthus	CN	69	900	35	31	r_c	−19	72	−
O. mniszechi‖	CN	70	800	34	32	r_c	−16	68	−
Oniticellini									
Euoniticellus intermedius	D	30	290	18	16	23	−8	0	+++
E. pallipes‖	D	33	320	18	16	23	−7	0	+++
Oniticellus planatus	D	44	320	20	17	20	−15	66	+++
Onitini									
Chironitis sp.	D	48	500	22	21	30	−13	64¶	++
Onitis alexis‖	C	44	750	33	32	57	−11	65¶	+
O. aygulus‖	C	51	1000	35	33	69	−13	>90	−
O. deceptor	C	64	1000	32	29	r_c	−11	71	−
Bubas bubaloides	DC	60	750	35	32	50	−11	65¶	++
Megalonitis bohemani	N	89	1500	33	30	r_c	−19	72	−
Coprini									
Catharsius tricornutus	N	52	900	(27)	24	r_c	−22	54	−
Copris fallaciosus‖	N	86	850	(30)	27	r_c	−23	37	−
C. hispanus	N	92	870	(32)	30	r_c	−28	38	−
Heliocopris japetus	N	164	2200	(27)	24	r_c	−15	26	−
Scarabaeini									
Sisyphus spinipes‖	D	36	320	22	21	40	−10	>90	+++
Garreta nitens	D	49	1050	26	25	44	−10	>90¶	++
Scarabaeus sacer	D	111	1300	30	26	r_c	−10	60	−
S. satyris	N	50	1000	30	27	r_c	−11	73	−
Kheper prodigiosus	N	99	1350	30	27	r_c	−11	64	−
K. nigroaeneus	D	74	650	28	26	46	−16	>90¶	+++
Pachylomera femoralis	D	122	1150	27	24	36	−11	>95	+++
Pachysoma schinzi	FD	102	1730	29	24	30	−11	>90¶	++

Values in parentheses are obtained from corneal geometry, as the outer facet margin is not discernible (see, for example, figure 8).

† Ventral eye region used only.

‡ D, day; C, crepuscular; N, night flying; F, flightless.

§ The more crosses, the greater the amount of screening pigment present.

‖ Fresh material.

¶ Pigment neutralizes lens cylinder at distal end.

PHILOSOPHICAL TRANSACTIONS OF THE ROYAL SOCIETY B BIOLOGICAL SCIENCES

such as *Cetonia* and *Diaphonia* (table 2), many small rutelines such as *Hoplia* and *Phyllopertha*, and in dung beetles of various sizes (the small members of the Oniticellini (table 3) and the large *Kheper nigroaeneus* (figure 13)). The common feature of these species is that they are active in the daytime. Many crepuscular species have slight curvatures to the outer facet surface. In the Oniticellini (Meyer-Rochow 1978) and Onitini, the facets of the dorsal region of the eye have considerably less individual curvature than those of the ventral eye region.

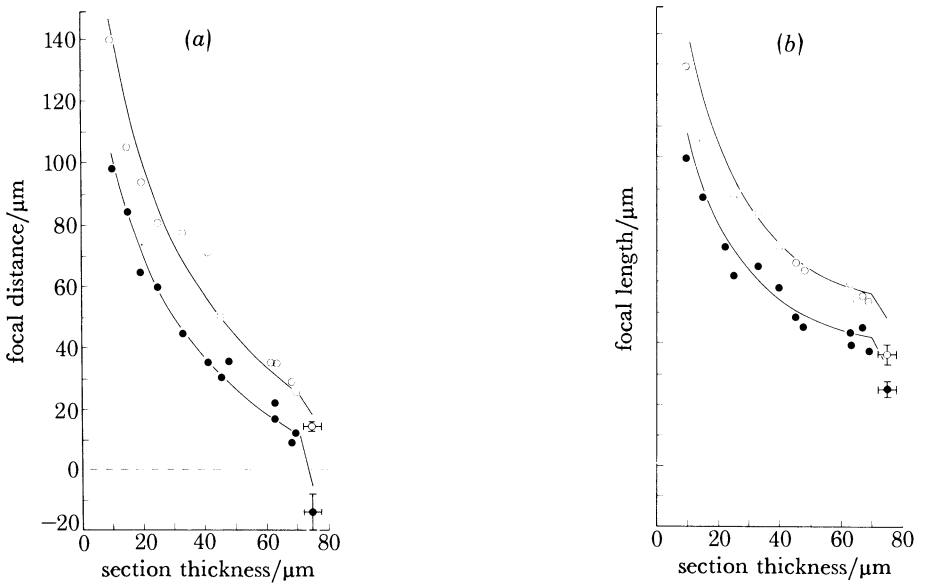

FIGURE 7. Focal distances (*a*) and focal lengths (*b*) of corneal slices from *Anoplognathus*. The focusing power of corneal cylinders differing only in length may be compared by shaving off tangential slices of cornea. All slices used included the outer corneal surface. The open circles refer to the focal distances (s') and lengths (f') in the back focal space ($n_2 = 1.337$) for orthodromic illumination, and the solid circles to the focal distances (s) and lengths (f) in the front focal space ($n_1 = 1.000$) for antidromic illumination. The focal distances and lengths of the intact lens ($t = 75$ μm) are also given (mean ± s.d.). It is obvious that the power of the corneal facet is a function of its thickness.

The lines fitted to the experimental points were generated by the generalized g.r.i. lens model (figure 3). Parameter values used were: $r_1 = 1000$ μm; $r_2 = -40$ μm; $r = 13.5$ μm; $n_0 = 1.54$; $n_b = 1.505$. A close agreement between experiment and theory is seen. The corneal lens cylinder appears to be fairly uniform in optical properties along its length. The intact lens ($r_2 = -11$ μm) has only slightly shorter focal distances than predicted by the model (*a*), although there was a considerable discrepancy between the focal lengths obtained by experiment and theory (*b*) for the intact corneal lens. This is most likely due to the inherent inaccuracies (10–20%) in our measurement of the image size from which the focal lengths were calculated. The image formed by the intact lens had a linear dimension of less than 4 μm in this species. The horizontal dashed line in (*a*) emphasizes the fact that the front focal plane is only inside the cornea when it is intact.

(*c*) *The corneal lens cylinder*

Cardinal-point analysis of corneal slices

Since a thick cornea precludes a strong front curvature to the individual facets, the power of the lens must reside elsewhere. In 1885, Exner showed that the cylindrical corneal facet of the water beetle *Hydrophilus piceus* (which has a flat front surface) remained a strong lens even when truncated by the removal of the rounded inner tip. He concluded that the water-beetle facet was a lens cylinder. Recently, Meyer-Rochow (1975, 1977, 1978), on the basis of interference microscope analysis of corneal sections, has reported that lens cylinders are not developed in the cornea of several scarab species. Nevertheless, the existence of a lens cylinder in the scarab

cornea can be demonstrated in a rather direct fashion by determining the cardinal points of tangential corneal slices. This was done for *Anoplognathus* spp. and *Geotrupes spiniger* with basically similar results.

A total of 12 tangential sections was cut from the corneas of nine specimens of *Anoplognathus*. The sections were floated on a drop of saline. All sections included the flat outer margin of the corneal facets. Front and back focal distances were measured with on-axis light and focal lengths calculated by the image magnification method. Sections ranging from 10 to 70 μm in thickness and the intact cornea (75 μm) were analysed. The data are plotted in figure 7*a*, *b*. What is immediately obvious in the lens of this genus is that its focusing power is a function of cylinder length. The values obtained experimentally from the truncated lens cylinders fit rather well the theoretical curves for a g.r.i. lens cylinder, as described in §2*e*. (The details of this model are given in figure 3.) The discrepancy between the predicted focal lengths for the intact lens and values obtained from image magnification (figure 7*b*) is probably due largely to the inherent inaccuracies in this method. This is especially true when the image is small, as it was for most intact corneal lenses analysed.

One drawback in this procedure was that the back surfaces of the corneal slices were not completely flat. As the razor-blade edge sheared the cornea, the shear plane often followed the curvature of the corneal lamellae. Consequently, individual cylinders had a convex back curvature of radius *ca.* −40 μm. This has been allowed for in the theoretical curves fitted to the experimental points in figure 7*a*, *b*. It is important to note that this back curvature was not always present and by itself cannot account for the refracting power of the corneal slices.

In *Geotrupes*, a slightly different approach was taken. Instead of cutting tangential sections of the cylinders, shallow wedges were cut. In these the inner surface of the sections displayed no individual facet curvature. Another advantage of this method was that a series of cylinders of different thickness could be examined in a single section. In *Geotrupes*, too, although the individual facets have a considerable front curvature, the focusing power of the lens is a function of cylinder length. Even when the refracting powers of the front and back surfaces of the cornea were neutralized by immersing the lens in oil ($n = 1.515$), a strong internal lens remained. The relative focusing power of the *Geotrupes* lens cylinder is not as strong as that of *Anoplognathus*.

Interference refractometry

In longitudinal sections of the corneal facets, the presence and extent of the g.r.i. lens cylinder (region b in figure 4) can be established in the interference microscope. The corneal lens cylinder is developed to varying degrees in different scarabs. In the cornea of most moderately sized species, a uniform radial g.r.i. lens (where n_0 and n_b, the r.i. on the axis and at the edge of the corneal lens cylinder respectively, and consequently their difference, Δn, remain constant along the length of the cylinder) is seen. The lens cylinder extends from the proximal margin of the cornea and terminates close to its distal margin. The outermost region of the cornea is homogeneous in r.i. (figure 4).

In many larger species, however, a considerable proportion of the distal cornea may be homogeneous and the lens cylinder confined to the proximal portion of the cornea. In these beetles, the proportion of the corneal facet that forms a lens cylinder may vary between 75 and 25% of the total facet length (figures 8, 9, 11; tables 2, 3). The obvious function of this design feature is to further reduce the refracting power of the distal region of the cornea.

The radial r.i. gradient in the lens cylinder of *Anoplognathus* was examined quantitatively in

PHILOSOPHICAL TRANSACTIONS OF THE ROYAL SOCIETY B BIOLOGICAL SCIENCES

the interference microscope. In longitudinal sections the lens cylinder appears to run three-quarters of the length of the corneal facet. In transverse sections through the lens cylinder, characteristic concentric interference fringes are observed (figure 14, plate 1). By measuring the r.i. profile in transverse sections from different points along the cylinder axis, the r.i. distribution along the lens cylinder can be constructed (figure 15). As might be predicted from the axial section of the lens cylinder, the outermost 20 μm of the cornea is virtually homogeneous, but the lens cylinder rapidly develops to give a value for Δn of 0.035 that persists to the proximal margin of the cornea. This r.i. gradient is achieved by a drop in marginal r.i. (n_b); the axial refractive index (n_0) remains constant.

In the vast majority of species examined qualitatively, the axial refractive index of the facet, and the lens cylinder where developed, appeared constant. In other words, the r.i. index of the distal homogeneous region of the cornea extends down the axis of the lens cylinder, as seen in *Scarabaeus sacer* (figure 9) and *Anoplognathus*. In two cases, however, the axial r.i. of the corneal cylinder was not constant. In all four coprine species examined (these having the least developed corneal lens cylinder (table 3)), the axial refractive index in the proximal lens cylinder was higher than that of the distal homogeneous region in the cornea (figures 8, 11). In *Trox*, although a well developed lens cylinder is present, both the axial and the marginal refractive indexes drop gradually in a proximal direction. This gives the appearance of strongly tapered lens cylinders, although the corneal facet cylinders are themselves almost parallel-sided.

(*d*) *The proximal corneal cone*

A convex, typically hemispherical, projection is seen at the proximal margin of the corneal facet. This 'corneal cone' is particularly well developed in *Geotrupes spiniger* (figure 10) and least evident in coprine species such as *Copris hispanus* (figure 11). In many species this cone has a tapered distal region and a round proximal tip (e.g. in *Bubas bubaloides* (figure 12) and in an extreme form in the immature passalid (figure 16)). Consequently, the radius of curvature of the tip is frequently less than half the proximal diameter of the facet (table 3). A corneal cone with this shape was illustrated by Grenacher (1879) for the cockchafer, *Melolontha vulgaris*.

The corneal cone is an important element of the corneal lens. In the cone the r.i. drops steadily from the centre of curvature to its curved edge, forming a hemispherical g.r.i. lens. *In situ*, the refracting power of the curved back surface of the cone (but not that of the g.r.i. lens) is neutralized by its close apposition to the (typically) concave front surface of the crystalline cone. Consequently the internal g.r.i. lens provides most of the refracting power of the proximal corneal cone. By placing a strong hemispherical g.r.i. lens at the proximal end of the lens

Description of plate 1

Figures 8–14. Interference micrographs of corneal sections. All micrographs are at the same magnification. (Magn. × 1000.)

Figure 8. *Heliocopris japetus*, l.s. cornea.

Figure 9. *Scarabaeus sacer*, l.s. cornea.

Figure 10. *Geotrupes spiniger*, l.s. cornea.

Figure 11. *Copris hispanus*, l.s. cornea.

Figure 12. *Bubas bubaloides*, l.s. cornea.

Figure 13. *Kheper nigroaeneus*, l.s. cornea seen in bright-field illumination. Extensive red-brown pigment lines the corneal facets.

Figure 14. *Anoplognathus* sp., wedge-shaped transverse section through the corneal lens cylinders. This section is thinnest at the lower right.

PHILOSOPHICAL TRANSACTIONS OF THE ROYAL SOCIETY B BIOLOGICAL SCIENCES

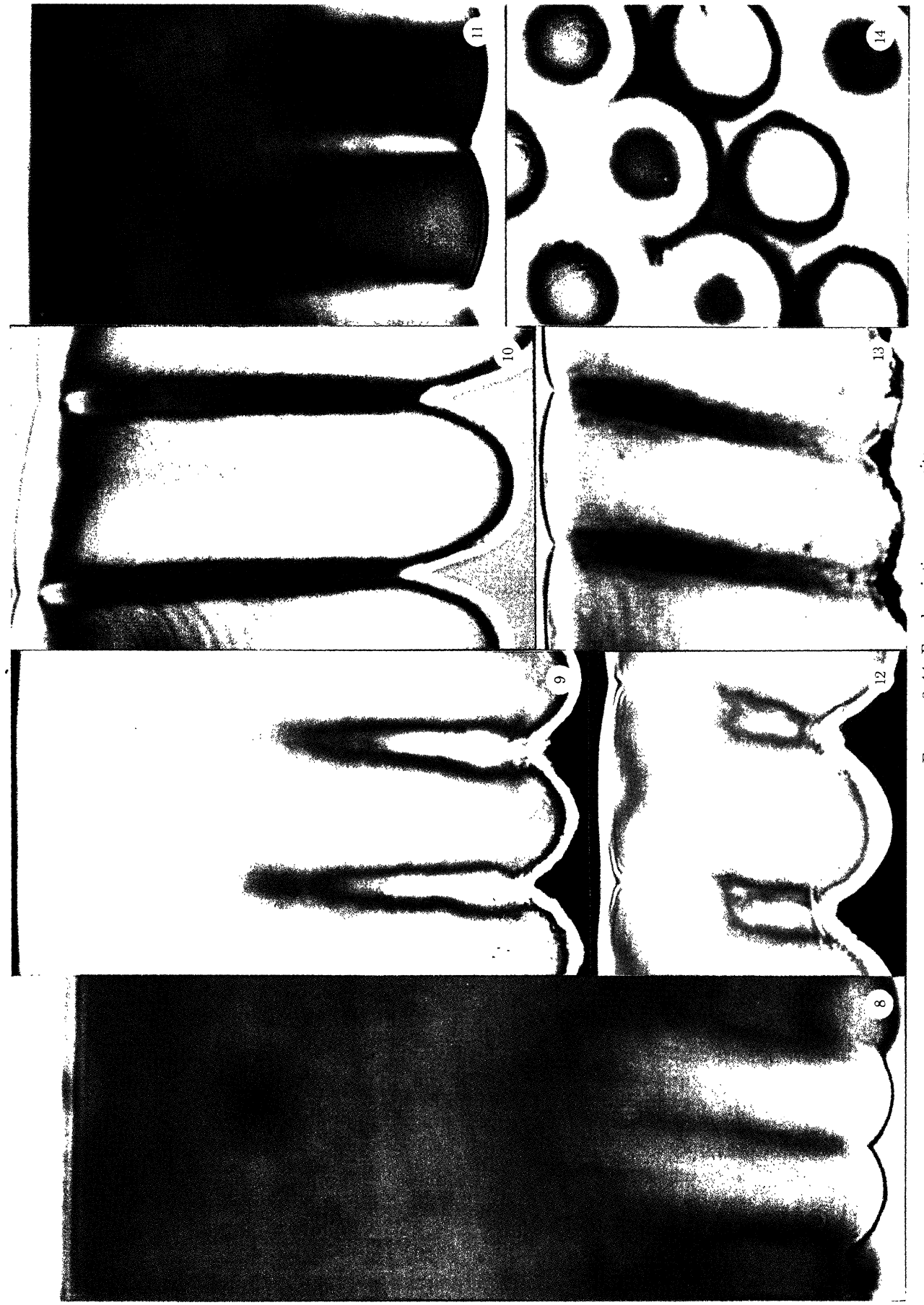

FIGURES 8–14. For description see opposite.

(*Facing page* 608)

PHILOSOPHICAL TRANSACTIONS OF THE ROYAL SOCIETY B BIOLOGICAL SCIENCES

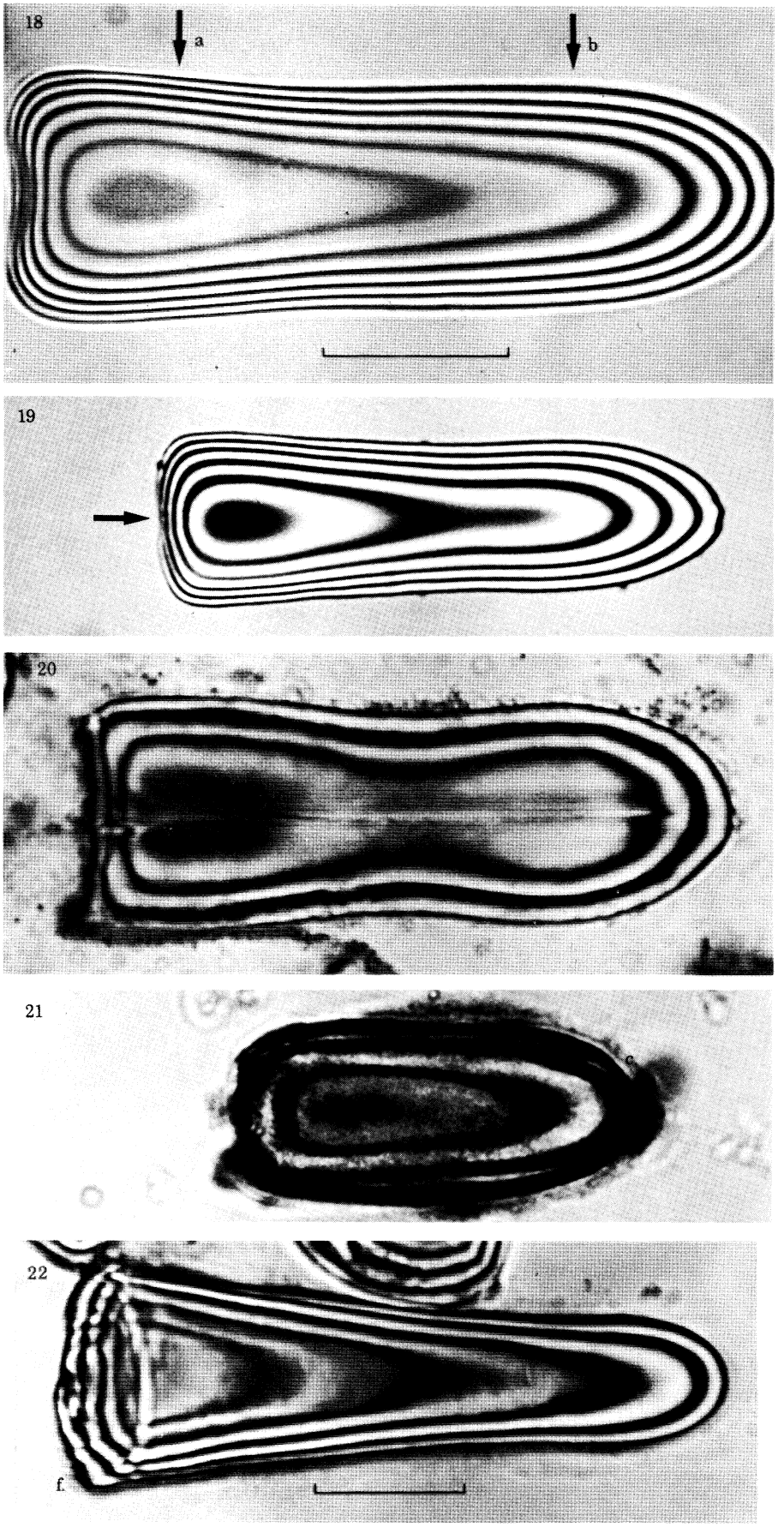

FIGURES 18–22. For description see opposite.

PHILOSOPHICAL TRANSACTIONS OF THE ROYAL SOCIETY B BIOLOGICAL SCIENCES

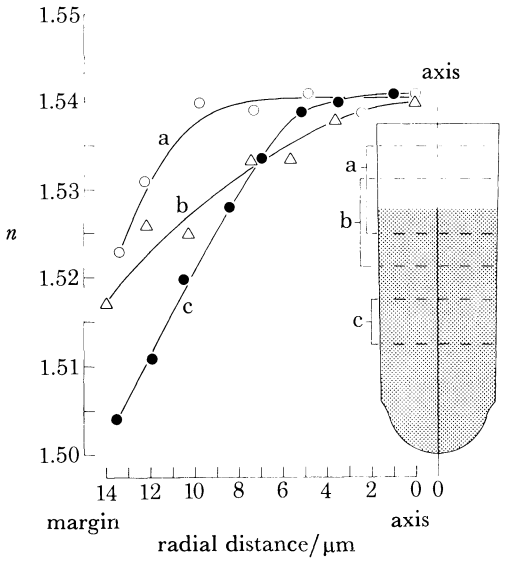

FIGURE 15. R.i. distribution across the corneal lens cylinder. The r.i. of the corneal lens cylinder in *Anoplognathus* is highest at the cylinder axis, declining towards the cylinder margin. The r.i. profiles across transverse sections of the lens cylinder at three different axial levels indicate that the profile is shallowest at the distal end of the lens cylinder (curve a) and steepest at the proximal margin (curve c). The inset shows a longitudinal section of the lens cylinder indicating the level and thickness of the three transverse sections analysed. The stippled area is the region of the lens known to have g.r.i. lens properties from qualitative examination of longitudinal sections.

cylinder, the principal planes of the lens are shifted proximally and the back focal point brought up close to the back surface of the cornea (figure 6).

The convex tip of the proximal corneal cone also serves to locate the (typically) concave distal surface of the crystalline cone. This inherently precise mechanism ensures the coaxial alignment of the two lens elements in the ommatidium.

(*e*) *The corneal process* (*exocone*) *of the passalid eye*

The corneal extension of the passalid beetle (and that of the bolboceratines and *Pleocoma* (table 2)) is so strikingly different from that of all the other scarab families that it deserves

DESCRIPTION OF PLATE 2

FIGURES 18–21. Interference micrographs of crystalline cones. Although the crystalline cones are transparent, they acquire characteristic interference fringe patterns when viewed in the interference microscope (λ = 546 nm). The ellipsoidal proximal tip of the cones faces the right. The scale bar (20 μm) applies to all four micrographs. The cones were immersed in saline.

FIGURE 18. Bullet-shaped cone of *Onitis aygulus*. The two vertical arrows indicate the axial levels at which the r.i. profiles plotted in figure 24 (curves a, b) were measured. The concave distal end of the cone may help to locate the cone against the back surface of the cornea (figure 17*a*), thus facilitating coaxial alignment of the lens elements. Fresh material.

FIGURE 19. Skittle-shaped cone of *Copris fallaciosus*. A slight waist is present. The slight dimple at the distal cone surface (horizontal arrow) again may help locate the cone against the back surface of the cornea. Fresh material.

FIGURE 20. Skittle-shaped cone of *Kheper prodigiosus*. Remnants of the cone cells adhere to the cone at the lower left. Alcohol-fixed material.

FIGURE 21. Bullet-shaped cone of *Geotrupes spiniger*. This cone is poorly developed with a granular texture. The cone is completely ensheathed in the cytoplasm of the cone cells (c.). Fresh material.

FIGURE 22. The corneal exocone of *Aulacocyclus endentulus*. The fracture face at which this exocone has broken away from the cornea is clearly evident (f.). The exocone has a slight waist. The cone, immersed in glycerol, appears to have undergone slight shrinkage. (Scale bar 20 μm.)

PHILOSOPHICAL TRANSACTIONS OF THE ROYAL SOCIETY B BIOLOGICAL SCIENCES

particular mention. The compound eye of the Australian passalid *Aulacocyclus edentulus* is large and hemispherical and has a glassy outer surface. In the immature adult (identified by its golden-brown colour, unlike the black of the mature adult) the cornea has not reached its ultimate thickness and the back surface of each lens has a sharply tapered cone that ends in a rounded tip (figure 16*a*). There is no crystalline cone, although at this stage of development

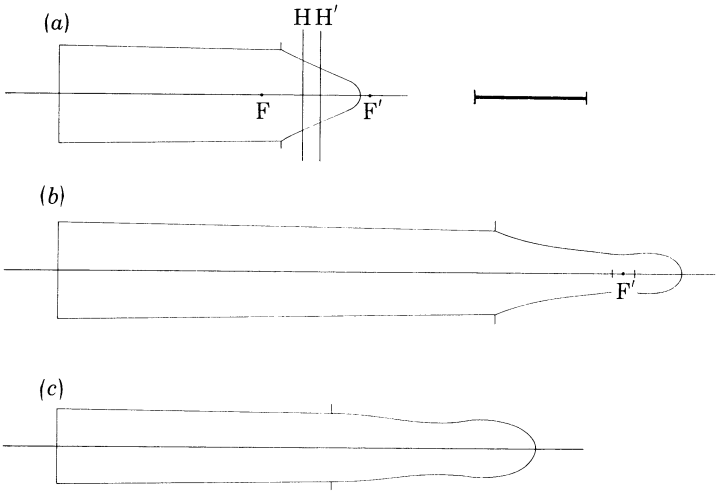

FIGURE 16. The passalid corneal exocone. In the cornea of the immature adult (*a*), no exocone projection is present, and the back focal point (F′) lies behind the lens. As the adult matures, the cornea almost triples in thickness and the back focal point now lies within the waist region of an exocone (*b*). For comparison, the corneal exocone of the click beetle *Pseudotetrolobus* is shown (*c*). Scale bar, 50 μm.

the back focal point of the lens cylinder lies outside the cornea (figure 16*a*) and a clear zone is present. As the adult matures, this conical projection of the lens continues to grow, until, in its completed state, the cornea is about 280 μm in thickness, and the back focal point lies *inside* the corneal projection (figure 16*b*). This passalid corneal cone bears a strong resemblance to the 'exocone' (Grenacher 1879; Kirchhoffer 1908) that has been described for the clear-zone eyes of fireflies and click beetles (Exner 1891; Seitz 1969; Horridge 1975). The cornea and corneal cone of the large Australian click beetle *Pseudotetrolobus* sp. (38 mm) is shown in figure 16*c* for comparison. It would appear that a functional exocone is present in both groups.

In a cleared corneal preparation from a mature adult the focal point within the cornea is not visible. By gently shaving off the proximal tips of the exocones, a sharp internal focus becomes visible and is found to lie between 20 and 30 μm from the proximal tip of the intact cone. A close examination of the exocone reveals that it has a distinct waist here that separates the distal tapered region from a bulbous tip with an elliptical back surface (figure 22, plate 2); the firefly cone also displays these morphological features (Seitz 1969). The presence of an internal focus in this flat-front-surface cornea clearly requires the development of a g.r.i. lens. Interference microscopy reveals a strong lens cylinder in the exocone projection.

The exocone compound eye would appear to have evolved entirely independently in at least two unrelated groups of beetles.

(*f*) *Corneal screening pigment*

The margins of the corneal facets in many day-active insects are lined with brown or black pigment. In the tiger beetle *Cicindela*, only on-axis light incident near the centre of the facet is

transmitted; light entering near the facet margin or at oblique angles is absorbed by this screening pigment (Friederichs 1931). The corneal facet has a non-adjustable iris diaphragm in such species.

A common feature in the cornea of the geotrupine and scarabaeine dung beetles, and cetoniine chafers, too, is the presence of fixed sclerotin-like pigment in the interfacetal region between the lens cylinders. A general rule is that this screening pigment is present in the corneas of diurnally active species, but absent in the nocturnal ones. For example, in the dung-beetle genera *Onthophagus*, *Onitis*, *Scarabaeus* and *Kheper*, the corneal lenses display extreme dimorphism: diurnal members have corneal screening pigment, but in nocturnal species this pigment is completely absent (table 3). In the diurnal *Kheper nigroaeneus* the pigment extends the full length of the lens cylinder (figure 13); in the Onitini it is restricted to the distal end of the cylinder (figure 12). Associated with heavy screening-pigment deposits is the presence of individual front curvature to the facets (table 3). The stronger the faceting, the heavier the pigment deposit. Screening pigment was never observed in the distal cornea of any scarab species in which the facets lacked individual curvature (table 3). No exocone eye examined had corneal screening pigment, although in the diurnal species *Stenaspidius albosetosus* the facets have strong individual curvature (table 2).

The function of the screening pigment found in the corneas of many diurnal dung beetles and chafers may be to filter out off-axis and stray light and, in conjunction with the strong front curvature to the facets (table 3). The stronger the faceting, the heavier the pigment faceting, light refracted at the outer surface of one facet but passing internally into an adjacent corneal lens cylinder would degrade the image formed by the corneal lens.

In several species (table 3) the high r.i. of the screening pigment, by spreading into the cylinder, may neutralize the corneal lens cylinder in the distal corneal region (figure 12). In *Garreta nitens*, the r.i. of the distal interfacetal pigment is greater than that on the cylinder axis, creating an inverted lens cylinder in this region. Whether this has any biological significance is unknown.

(*g*) *Primary image quality, reduction in facet diameter and facet tilt in diurnal species*

In comparing the optical properties of the isolated corneas from many species, considerable variation in the sharpness of the primary image in orthodromic illumination was noted. The corneal lens cylinders of crepuscular and nocturnal dung beetles, and the passalid exocone, focused very sharp images, while the lenses of diurnal scarabs often gave very poor images.

Image quality appears to be strongly correlated with corneal lens diameter. In our survey of the lamellicorns, facet diameters ranging between 18 and 41 μm were recorded. Corneal facets are smallest in the eyes of species active in the day, but considerably larger in closely related crepuscular and nocturnal species (table 3). For example, in the diurnal Onthophagini ϕ_d ranges between 17 and 23 μm, whereas crepuscular and nocturnal species have a ϕ_d between 26 and 35 μm. A similar trend is evident in the Onitini and Scarabaeini (table 3). In the Oniticellini, a mainly diurnal group, the facets are very narrow. Overall, narrow facets lined with corneal screening pigment gave the worst images. Since the presence of screening pigment further reduces the effective diameter of the facet it is likely that the poor images seen in these eyes are the result of diffraction effects. Although a narrow facet gives larger diffraction effects than a wider facet, it does have an increased depth of focus (and hence tolerance to other lens aberrations). The exit pupil of the dioptric system, the crystalline cone tip, also has a narrower

PHILOSOPHICAL TRANSACTIONS OF THE ROYAL SOCIETY B BIOLOGICAL SCIENCES

diameter in diurnal scarabs, due either to cone size or tip aperture created by an annulus of screening pigment (see §5), that may be matched to the facet diameter. The greater facet diameter in nocturnal species may represent an attempt to reduce the diffraction limitation of the corneal lens cylinder in these species.

In many species a non-radial orientation of the ommatidial (and corneal lens-cylinder) axis relative to the eye surface was seen. This facet 'tilt' was most noticeable in diurnal species with a heavy deposit of screening pigment in the cornea (such as *Kheper nigroaeneus* (figure 13)), especially in the dorsal region of the eye. In this region, more facets 'point' in an anteriodorsal direction than would be expected if the eye had spherical symmetry. Departure from spherical symmetry in superposition eyes will improve local resolution in the eye, but will downgrade the image elsewhere (Land *et al.* 1979). It is interesting to note that tilted lens cylinders are rarely seen in night-flying species, but are common in day-flying ones. Since beetle ommatidia may function in the apposition state during the day, regions of tilted facets may be analogous to the acute zones (Horridge 1978) seen in the permanent apposition compound eyes of other arthropods.

5. Crystalline cone design

Directly beneath the corneal facet in the typical scarab compound eye is a solid and transparent crystalline cone. It forms the second dioptric element in the eye and is a strong g.r.i. lens (Meyer-Rochow 1975). This crystalline cone is of the 'eucone' type (Grenacher 1879), being the combined intracellular secretions of four tightly apposed cone cells. With the exception of the passalid beetles, where the eucone is replaced by its functional analogue the corneal exocone, and some lucanids, where the crystalline cone is lacking, all scarab eyes appear to be of this eucone type. According to superposition theory, the crystalline cone and the corneal lens together form an afocal lens pair; the distal crystalline cone combines with the corneal lens to give an intermediate image within the cone, and the proximal cone tip projects this image across the clear zone onto the retina (Exner 1891; Horridge 1975). Although the general morphology of the crystalline cone varies considerably in different species, the ellipsoidal shape of the proximal tip is highly conserved. This ellipsoidal surface encloses a g.r.i. lens that can be envisaged as a series of ellipsoidal shells with refractive index decreasing towards the surface (see figure 5). The refracting power of the proximal cone tip lies in this internal r.i. gradient rather than in its ellipsoidal surface, which has a r.i. similar to that of the surrounding medium.

The ability of the crystalline cone to focus light onto the receptor layer will depend largely on the position of the intermediate focus within the cone. If the corneal g.r.i. lens and the distal crystalline cone focus the image too near the cone tip, the light will diverge on entering the clear zone. If the intermediate focus is located too distally, the light will converge in the clear zone, then diverge. In both instances the quality of the superposition image will be reduced (see §6*a*).

In examining the imaging qualities of the scarab eye, it is therefore important to establish the precise position of the intermediate focus in the crystalline cone. That it is within the cone was first demonstrated directly for the water beetle *Hydrophilus piceus* by examination of fresh eye slices in which the crystalline cones were left *in situ* (Exner 1876). An image of an object placed at infinity is seen within the cone. In examining several scarab species, we measured the apparent distance of the image distal to the cone tip as 10–20 μm. In *Anoplognathus*, the apparent distance was 12 μm. It was not, however, easy to obtain this measurement. Furthermore, we

PHILOSOPHICAL TRANSACTIONS OF THE ROYAL SOCIETY B BIOLOGICAL SCIENCES

have not attempted to calculate the real depth of the image within the cone from these data, since this involved a correction for the refracting power of the back elliptical surface of the cones and the r.i. distribution within the cone. It is possible, nevertheless, to obtain a reasonably precise estimate of the image position from theoretical predictions and indirect observations on the following:

(i) cone morphology, in particular the presence of a constriction (waist) in the crystalline cones of many beetles;

(ii) the position of the back focal point of the cornea when the r.i. in the image space matches that on the axis of the crystalline cone;

(iii) the distribution of mobile screening pigment around the crystalline cone;

(iv) the position of the focus in the corneal cone of the passalids; this focal point can be measured directly (§4*e*); the corneal cones of exocone eyes bear a strong anatomical resemblance to the crystalline cones of many scarabs;

(v) the position of the internal focus can also be predicted from a model of the proximal tip of the crystalline cone in which the shape and r.i. distribution in the cone are considered.

Items (i)–(iii) and (v) will now be discussed in detail. Item (iv) has already been treated in §4*e*.

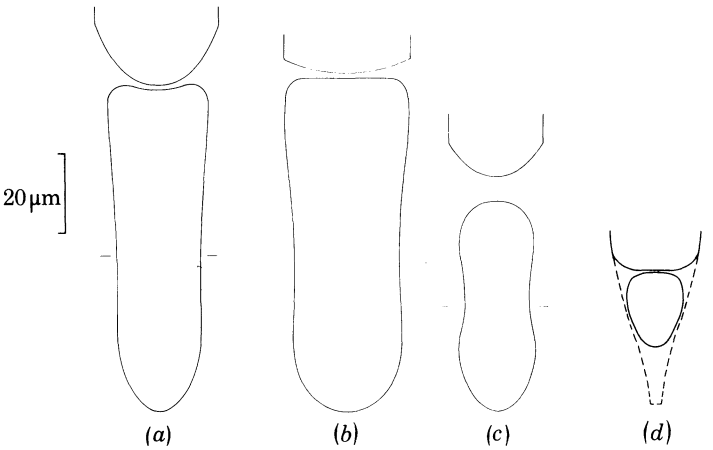

FIGURE 17. The four main crystalline-cone shapes. (*a*) Bullet-shaped cone (*Onitis aygulus*). (*b*) Skittle-shaped cone (*Onthophagus pentacanthus*). (*c*) Hourglass-shaped cone (*Pachysoma schinzi*). (*d*) Pear-shaped cone (*Phyllopertha horticola*). The cones are all drawn to the same scale. The position of the proximal tip of the corneal lens cylinder relative to the crystalline cone is also shown. The position of the cone waist is indicated by the short horizontal lines. The outline of the cone cells is indicated by the dashed lines in (*d*).

(*a*) *Crystalline cone morphology*

The overall similarity in shape of the crystalline cone in the eyes of many arthropod species thought to employ refracting superposition optics is 'uncanny' (Land *et al.* 1979); presumably it reflects a common design principle. Considering the optical importance of the crystalline cone to superposition image formation, this is hardly surprising. It is, however, remarkable that the precise shape of the beetle eucone, although accurately drawn by Exner (1876), one of the few early authors to comprehend its optical function, and Schultze (1868), has been so erratically portrayed and contested in many recent papers. The problem appears to have arisen because the overall appearance of the crystalline cone is related to the daily activity pattern of the species involved. In the eucone eyes of Lepidoptera, for example, the crystalline cone of

PHILOSOPHICAL TRANSACTIONS OF THE ROYAL SOCIETY B BIOLOGICAL SCIENCES

diurnal butterflies is often strongly tapered or pear-shaped; in nocturnal moths the crystalline cone has a cylindrical body and resembles an artillery shell (Friederichs 1931). In both cases the cones have a rounded tip.

In scarabs, too, the considerable variation in cone shape can be correlated with diel activity. Although the proximal tip of the crystalline cone in all species examined has an elliptical profile, the remainder of the cone shows a continuum of shapes that can be divided, somewhat

Table 4. Crystalline cone and corneal exocone dimensions

species	flight activity	cone shape	L µm	distal end ϕ_d µm	waist distance from tip µm	waist ϕ_w µm	proximal tip ϕ_p µm	proximal tip ellipticity, y_b/x_b
(*a*) crystalline cones (ranked according to size)								
Onitis aygulus	CN	bullet	84	26	(40)†	(23)	23	0.58
Onthophagus pentacanthus‡	N	skittle	82	30	36	25	26	0.72
Kheper prodigiosus‡	N	skittle	72	28	36	23	25	0.63
Copris fallaciosus	N	bullet	69	23	(30)	(20)	20	0.53
Pachysoma schinzi‡	FD	hourglass	53	18	27	16	19	0.56
Kheper nigroaeneus‡	D	hourglass	51	22	26	14	18	0.86
Anoplognathus spp.	C	bullet	49	18	(26)	(14)	13	0.54
Onthophagus taurus	D	pear	45	16	–	–	11	–
Geotrupes spiniger	CN	bullet	41	15	–	–	13	0.65
Phyllopertha horticola‡	D	pear	19	14	–	–	–	–
Lamprima aurata‡	D	ovoid	10	7	–	–	–	–
(*b*) corneal exocone								
Aulacocyclus edentulus	N	skittle	85	35	24	23	24	0.60

† Values in parentheses are estimates, as no distinct waist is present in the bullet-shaped cone.
‡ Alcohol-preserved material.

arbitrarily, into four main types. These types are based on the shape of the distal (front) surface (convex, flat or concave), the waist (absent, slight or pronounced), and degree of cone taper (slight to very strong). By these three criteria, crystalline cones can be described as 'bullet-shaped', 'skittle-shaped' (both typically large cones and characteristic of crepuscular and nocturnal species), 'hourglass-shaped' and 'pear-shaped' (both smaller cones seen in diurnal species).

The *bullet-shaped cone* has a flat or slightly concave front surface that abuts the back surface of the corneal facet, and sides that taper distally but become cylindrical towards the ellipsoidal tip (figure 17*a*; figure 18, plate 2). A large bullet-shaped cone is typically seen in crepuscular or night-flying species with wide corneal facets (table 4) and was the type most frequently encountered in our survey. The proximal cone tip of the bullet-shaped cone varies in its ellipticity. In some species it is strongly elliptical (figure 17*a*) but in others it is less so. Cone size may show considerable variation, even among ommatidia of a single eye. In *Onthophagus mniszechi*, for example, nearby cones varied in length from 66 to 86 µm. The scaling of the cones, however, remained constant. In rutelines active in the daytime, a small bullet-shaped cone with a strong distal taper is commonly seen. In many geotrupines the crystalline cone, although bullet-like in shape, is poorly developed with a granular texture (figure 21, plate 2). The bullet-shaped cone ranged between 40 and 90 µm in length in species examined.

The *skittle-shaped cone* also has a flat or concave front surface, but the sides of the cone constrict

to form a slight waist (figure 17*b*). The proximal tip forms a wide ellipsoid. This cone shape is also common in large nocturnal species with wide facets. Its length ranges between 50 and 80 μm.

The *hourglass-shaped cone* possesses a strong waist and a hemispherical distal region (figure 17*c*). The proximal tip is ellipsoidal. This cone is restricted to diurnal dung beetles of the tribe Scarabaeini (table 4), the only previous citing being that of Kirchhoffer (1908) for *Scarabaeus variculosus* (=*S. variolosus* F.?). The hourglass cone is relatively small (40–50 μm) and associated with narrow facets (figure 17*c*). It is often set back away from the corneal back surface. Anatomically, the 'waist' in the skittle- and hourglass-shaped cones corresponds to a region in the larger bullet-shaped cones where the tapered and cylindrical sections meet (figure 17).

The *pear-shaped cone* is also small (less than 40 μm in length) and has a slight to strong convex front surface. The diameter of the distal region of the cone is considerably greater than that of its proximal region, and the cone tip forms a relatively narrow ellipsoid. The pear-shaped cone may be quite elongated (as seen in the dung beetle *Euoniticellus africanus* by Meyer-Rochow 1978). In *Phyllopertha horticola* the cone is very small and encased in strongly tapered cone cells (figure 17*d*). The pear-shaped cone is probably the type seen in other chafers, such as *Hoplia farinosa* L. and *Trichius fasciatus* L., although Kirchhoffer (1908) illustrates these two species as having pointed crystalline cones (rather than pointed cone cells). A lens with a pointed surface would scatter light. Scarabs with pear-shaped crystalline cones are active in bright sunshine.

Two other shapes of crystalline cone deserve brief mention. In the diurnal stag beetle *Lamprima aurata*, the cone is reduced to a small ovoid structure (table 4). For the nocturnal rhinoceros beetle, *Oryctes rhinoceros*, Bugnion & Popoff (1914) illustrate (p. 292) a large elliptical cone as well as a typical bullet-shaped cone split open to show its four segments. It is unclear which is the correct shape. In the rhinoceros beetle that we examined, *Dasygnathus*, the crystalline cone had a typical bullet shape.

To recapitulate, the crystalline cones in the clear-zone eyes of nocturnal scarabs are large with wide ellipsoidal tips. In end view, the cones of nocturnal species are tightly packed to allow maximum transmission of light. Diurnal scarabs have strongly tapered cones with smaller ellipsoidal tips that presumably transmit less of the light incident on the eye.

The shape of the waisted crystalline cone resembles that of the corneal exocone (figure 22) seen in some clear-zone eyes. As stated earlier, the intermediate focus in the exocone is at the level of the waist. As the corneal exocone is the functional analogue of the crystalline eucone, a similar point of focus is likely.

No adaptation in crystalline cone shape in scarab eyes was seen in response to ambient light intensity. In the gyrinid beetle *Macrogyrus*, the cone has an elliptical tip at low light intensities, whereas at high light intensities it has a long tapering point (Horridge 1976). Unlike the flexible cone of the gyrinid (personal observation) the scarab cone is rigid. The difference in cone shape in diurnal and nocturnal scarabs may then represent a permanent adaptation to extremes of light level.

(*b*) *The back focal distance of the isolated cornea*

We have already described the back focus of the corneal lens as lying close to the back surface of the cornea when the back focal space is filled with saline ($n = 1.337$). When this space is filled with fluids of higher r.i., this focal distance increases accordingly. It becomes slightly longer when albumin solutions ($n = 1.38$–1.42) replace the saline in the back focal space, and considerably longer when oil ($n = 1.515$) is used.

PHILOSOPHICAL TRANSACTIONS OF THE ROYAL SOCIETY B BIOLOGICAL SCIENCES

The corneal back focal distance in saline, albumin and oil is given for several species, and is compared with the corresponding crystalline cone length, in figure 23. It is obvious that this dimension of the crystalline cone is 'tuned' to the corneal back focal distance. Although the correlation is quite good when media of low r.i. are used, it becomes much stronger when the back curvature of the cornea ($n \approx 1.50$) is neutralized by the higher r.i. of the oil. *In vivo*, much

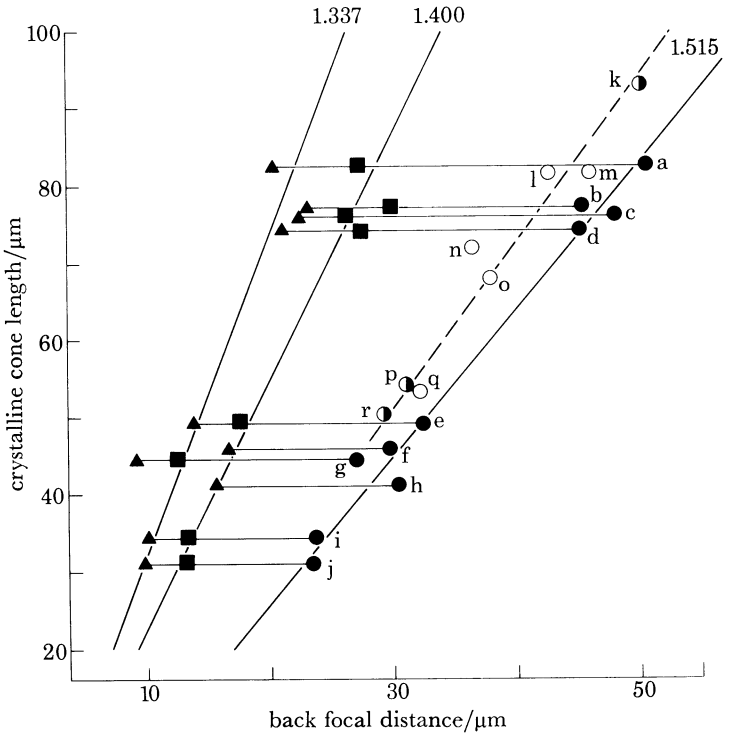

FIGURE 23. The relation between the back focal distance of the corneal lens when the cornea is floated in media of differing r.i., and the length of the crystalline cone. The back focal distance (s') of the isolated cornea was measured when saline ($n = 1.34$), albumin solution ($n \approx 1.40$) and oil ($n = 1.515$) successively filled the back focal space. The horizontal lines connect the values for s' measured in saline (▲), albumin solution (■), and oil (●) for each preparation. Each set of values is plotted against the average crystalline-cone length from the same region of the eye. The species examined were: *Onitis aygulus* (a, b); *O. alexis* (c, d); *Anoplognathus* sp. (e); *Aphodius tasmaniae* (*f*); *Onthophagus taurus* (g); *Sisyphus spinipes* (h); *Euoniticellus pallipes* (i, j).

In addition, the distance between the corneal back surface and the plane of the crystalline-cone waist (abscissa) is plotted as a function of total crystalline-cone length (○). The crystalline cones were from *O. aygulus* (l); *Onthophagus pentacanthus* (m); *Kheper prodigiosus* (n); *Copris fallaciosus* (o); *Pachysoma schinzi* (q). Finally, the length of several corneal exocones (ordinate) is plotted against the waist distance from the distal limit of the exocone projection (◑: *Pseudotetrolobus* sp. (k); *Phausis* (*Lampyris*) *splendidula* (p), data from Seitz (1969); and *Conoderus* sp. (r)). The dashed line drawn through this latter set of points suggests that the distal crystalline cone or exocone is the optical equivalent of a homogeneous spacer of r.i. *ca.* 1.48.

of the refracting power of the corneal back surface (but not that of the internal g.r.i. lens) is neutralized by the abutment of the crystalline cone, as the crystalline cone has a central r.i. close to that of the proximal cornea (see §5*d*).

The position of the cone waist relative to the corneal back surface is also plotted in figure 23. The back focal point would lie in the waist region if the complex g.r.i. lens of the distal crystalline cone could be reduced to an optical spacer with r.i. of about 1.48 (dashed line in figure 23).

PHILOSOPHICAL TRANSACTIONS OF THE ROYAL SOCIETY B BIOLOGICAL SCIENCES

(*c*) *The distribution of mobile screening pigment around the cone*

In most scarabs, the crystalline cone is completely surrounded by a sleeve of screening pigment granules that leaves a small aperture open at the proximal tip. In the dark-adapted state most of the proximal ellipsoidal surface of the cone is free of pigment, but in the light-adapted state the pigment at the cone tip acts as a pupil and stops down to an aperture of 2 μm diameter or less (Horridge & Giddings 1971, fig. 7; S.C., personal observation). In the latter state a crystalline tract, also surrounded by pigment, is often present (Meyer-Rochow & Horridge 1975).

When waisted cones are examined, it appears that the waist contains a denser belt of pigment than elsewhere. In *Copris* (and other coprini), the screening pigment is completely absent from around the distal cone region and forms a layer extending from the waist to the tip of the cone. In *Pachysoma*, the pigment granules form a belt around the crystalline cone waist and a cap at the cone tip; the rest of the cone surface is free of pigment. The optimum position for such a lateral screening pigment to act as a field stop, restricting the angular acceptance of the ommatidial optics, would be at the intermediate focal plane, as all rays incident on the ommatidium at a given angle to the axis are brought to a common focus here (the larger the angle, the further the point of focus from the axis). Friederichs (1931) was quite wrong when he stated that the hourglass crystalline cone is a fixation artefact of no physiological significance. The waist, by removing rays at large angles to the axis of the ommatidium, restricts the number of ommatidia that may contribute to the formation of a superposition image. It thus determines the maximum aperture of the eye (figure 28). The fixed aperture of this field stop (i.e. waist diameter) is particularly narrow in diurnal species with hourglass cones, such as *Pachysoma schinzi* (figure 17*c*) and *Scarabaeus variolosus* (Kirchhoffer 1908). The function of waist in strongly waisted cones may be complemented by the corneal screening pigment that prevents light crossing between facets, as in several diurnal dung beetles and chafers.

(*d*) *Ray tracing through the proximal tip of the crystalline cone: a model*

It is possible to predict the intermediate focal point within the crystalline cone by modelling the back surface of the cone and its internal r.i. gradient. To do this realistically, the magnitude and profile of the r.i. gradient need to be obtained. In the few insects examined to date, the flour moth *Ephestia* (Hausen 1973), the water beetle *Cybister* (Meyer-Rochow 1973) and the scarab *Anoplognathus* (Meyer-Rochow & Horridge 1975), the eucone crystalline cone has been shown to be a cylindrical or slightly tapered g.r.i. lens.

The presence of a radial gradient in r.i. at any level along the crystalline cone axis can be demonstrated by the analysis of intact cones in the interference microscope. As the cones are cylindrical in cross section, the thickness at any point can be determined readily from geometry, and the average r.i. at that point calculated from the measured phase difference between the point and the surrounding fluid of known r.i. Double-immersion interferometry is not required. This method yields an accurate value for n_b but the r.i. for the central region is an underestimate (by 0.02–0.04) of the real axial r.i., since one is sampling the full range of r.i. values in the cone. Nevertheless, this method immediately reveals whether the lens is homogeneous in r.i. or not and whether the gradient is parabolic. (A parabolic actual gradient will give a parabolic measured gradient with a smaller central value and therefore a slower fall-off from centre to edge than the actual gradient.) R.i. scans at different axial levels of intact bullet-shaped cones from two species are shown in figure 24. *Onitis aygulus* has a large crystalline cone

PHILOSOPHICAL TRANSACTIONS OF THE ROYAL SOCIETY B BIOLOGICAL SCIENCES

(table 4) which was scanned across its maximum distal diameter (ϕ_d) and across the base of the proximal elliptical tip (ϕ_p, arrows in figure 18). The crystalline cone is not homogeneous, but has a higher r.i. in the centre than at the edge. At the distal end the r.i. is fairly constant over a wide central area, but then drops off abruptly at the edge (figure 24*a*). More proximally the r.i. profile shows a more gradual decline from axis to margin (figure 24*b*).

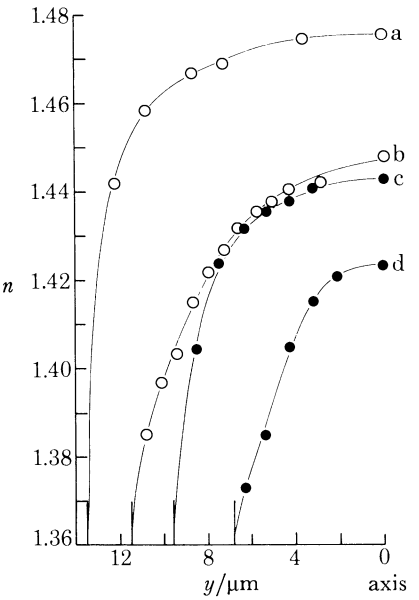

FIGURE 24. The r.i. profile across the intact crystalline cone. The crystalline cones of *Onitis aygulus* (○) and *Anoplognathus chloropyrus* (●) were each scanned at two axial levels. The cones were immersed in physiological saline. In *Onitis*, the r.i. profiles of the distal cone region (curve a) and the proximal cone tip (curve b) were calculated. In *Anoplognathus*, the distal region (curve c) and the waist region of the crystalline cone (curve d) were scanned. The abscissa (y) represents radial distance from the cone axis; the short vertical lines on this axis indicate the cone radius at the level scanned. These curves are very close to parabolic, with a slightly faster fall off near the edge of the cone.

This difference between the r.i. profiles of the distal and proximal regions is suggested by the different spacing of the interference fringes in these regions, as seen in figures 18 and 19, although it must be remembered that fringe spacing depends on the thickness of the cone (which obviously decreases towards the periphery), as well as on the r.i. gradient. That the difference in fringe spacing between the distal and proximal regions reflects a different r.i. profile and is not a thickness (i.e. different cone diameter) effect can be seen directly by comparing figure 24*b*, *c*: in the smaller crystalline cone of *Anoplognathus* spp., the r.i. in the distal region (figure 24*c*) has a more abrupt profile than that in the proximal region of *Onitis* (figure 24*b*), even though ϕ_d for *Anoplognathus* is less than ϕ_p for *Onitis* (table 4).

To obtain a precise value of n_0, sections of the cone are required. If the space around the cones in a fresh eye preparation is stabilized with gelatin, cross sections of crystalline cones may be cut with little difficulty by means of a sharp razor blade (Hausen 1973). In *Anoplognathus* a value of n_0 of 1.48 was obtained for the distal crystalline-cone region by this method. The r.i. drops off in an approximately parabolic manner to a marginal value between 1.36 and 1.38. A similar parabolic profile has been reported by Hausen (1973) in *Ephestia*. A radial g.r.i. lens cylinder with a parabolic profile in r.i. gives, in theory, the best focus for on-axis light when

there are no surface curvatures (Fletcher *et al.* 1954; Kapron 1970; Marchand 1978; the sech gradient of Fletcher *et al.* is equivalent to a parabolic gradient for the r.i. values considered here).

To test the focusing power of the proximal crystalline cone, a two-dimensional model (§2*e*) was constructed in which a g.r.i. lens cylinder terminated in a g.r.i. lens hemiellipse. This appears to be the preferred shape for superposition vision, since, as we have described, the proximal cone in crepuscular and nocturnal scarabs is invariably cylindrical, or near-cylindrical, and terminates in an ellipsoidal tip. The r.i. profile in both the cylindrical and elliptical regions was taken as varying with the square of the distance from the appropriate axis (as shown in figure 5). Values for the axial (n_0) and marginal (n_b) r.i. were selected from interference refractometry of actual cones described earlier. We reasoned that the cornea and distal crystalline cone together are capable of focusing a reasonably good image within the cone, and that the function of the proximal cone is to project this intermediate image across the clear zone onto the retina. According to superposition theory, the light rays leaving a cone, to contribute to an erect superposition image of a distant object, should be approximately parallel. Consequently, we initially studied the power of the proximal tip in reverse, i.e. we tested its ability to focus parallel light that entered the cone tip at various angles of incidence relative to the cone axis.

The focusing ability of the lens for meridional rays at varying angles of incidence is shown diagrammatically in figure 25. With the exception of the most peripheral rays, the model lens shows good ability to concentrate light to a point focus. These peripheral rays are presumably eliminated *in vivo*, except in the most dark-adapted state, by the variable-aperture exit pupil created by the mobile pigment at the cone tip. As a measure of the lens aberrations, the diameter of the geometric blur circle can be considered. Even at wide angles of incidence, the lens appears to be able to focus light to a blur circle less than 1 μm in diameter (but see below).

In the model shown in figure 25, the ellipse was given a value of $x_b = 11$ μm and $y_b = 6$ μm. For on-axis rays, this model focused light to a point 23–25 μm from the surface of the cone (figure 25*a*), with a best focus at 23.6 μm. Off-axis rays are focused at slightly shorter distances, rays incident at 20° being focused to a point 21–23 μm from the back surface of the cone (figure 25*d*). In an actual cone of this size (*Anoplognathus*) this focus falls in the waist region.

Although the absolute size of the crystalline cone varies in different species, the proportions of x_b and y_b remain fairly constant (table 4). Consequently, the position of the focus is scaled up or down accordingly and remains in the waist region of the cone, at a distance from the proximal cone tip of about twice x_b, irrespective of cone size (see methods). This explains the fact that neighbouring crystalline cones from a single eye may vary in scale by as much as 20%. If they have similar proportions, they achieve the same optical effect, provided that the intermediate focus formed by the corneal facet and distal crystalline cone lies at the waist.

A major factor in the quality of the superposition image is the spread in the light leaving the proximal tips of the cones (see discussion). In an ideal afocal system, light leaves a cone as a parallel beam, but in a real system, lens aberrations and diffraction at the aperture at the proximal cone tip tend to spread the beam. Reverse ray tracing (figure 25) indicates that lens aberrations (at least those of the proximal crystalline cone, the second component of the system) are small and that diffraction may be the dominant factor in causing beam spreading. To test this directly, rays were traced from a point at the on-axis position of the intermediate image (taken to be 23.6 μm distal to the proximal cone tip; figure 25) through the proximal cone and projected to where the rhabdoms lie (a range of distances 150–800 μm behind the cone tips). This was done for a range of aperture diameters, and the ray intensity distribution com-

PHILOSOPHICAL TRANSACTIONS OF THE ROYAL SOCIETY B BIOLOGICAL SCIENCES

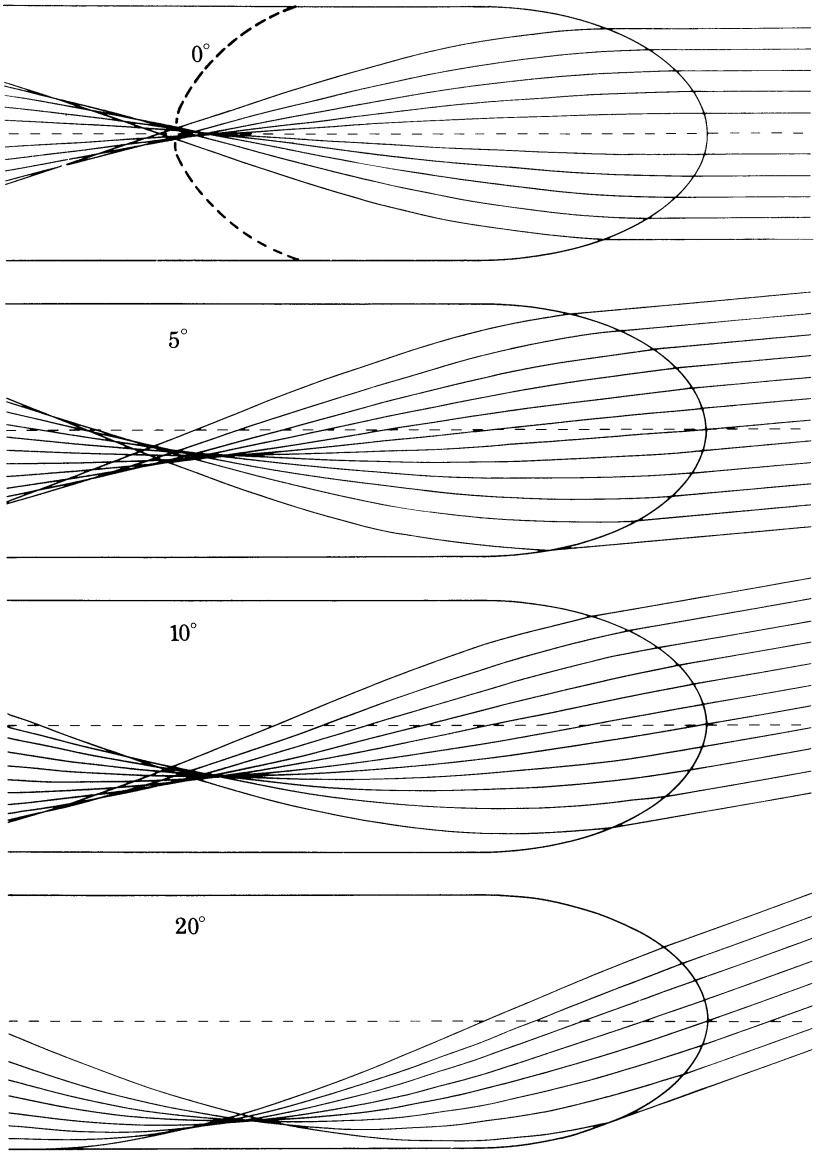

FIGURE 25. Ray tracing through a model g.r.i. crystalline cone at various angles of incidence. Based on data from *Anoplognathus*, the parameter values used are: $x_b = 11$ μm; $y_b = 6$ μm; $n_0 = 1.48$; $n_b = 1.36$; $n_s = 1.34$. The focus, which falls within the cylindrical region of the model g.r.i. lens, has a geometric blur circle of less than 1 μm in diameter. At values of θ much greater than 20° the focus will fall beyond the lens boundary. Note that the focal plane in this model crystalline cone is not flat but curved (dashed line in $\theta_i = 0°$ diagram). (A similar curvature is seen in the model of Cleary *et al.* (1977).) Since the ideal position for the marginal off-axis focus (θ_i slightly greater than 20°) would be at the cone waist, it follows that the on-axis focus may be several micrometres distal to this point.

pared with that arising from diffraction at the aperture. In all cases the spread due to diffraction was considerably larger than that due to lens aberrations, indicating that diffraction at the proximal cone tip is the limiting factor in the size of the blur circle formed by the proximal crystalline cone. This is true even for the largest crystalline cones examined, which had a maximum tip diameter ($2y_b$) of 26 μm (table 4).

6. Discussion

(a) *Image quality in the eye*

In an ideal superposition eye, collimated beams of light emerging from the cone tips of the contributing ommatidia exactly superimpose to form a small patch of light, the blur circle, at the level of the distal rhabdom tips. In a real eye the size of the blur circle will be larger than in the ideal eye because of the spread in the individual beams and because all the beams do not superimpose precisely. Spreading of individual beams is caused by aberrations of the afocal lens system and by diffraction at the limiting aperture of the ommatidium, while the beam will emerge from the cone tip at an incorrect angle if the ommatidial axis is misaligned or if the angular magnification of the afocal system is inappropriate to the clear-zone width (see Diesendorf & Horridge (1973) and Land *et al.* (1979) for a detailed discussion of this point).

It is difficult to observe the beam formed by an intact individual afocal system (i.e. a single ommatidium) because the crystalline cones are very easily dislodged from their position behind the corneal facets. However, while direct observational proof is lacking, it is possible, with use of the results of §5*d*, to estimate the spread of the beam. The aberrations of the afocal system can be analysed in terms of the aberrations of the two components and the effect of them not being afocal. As discussed in §5*d*, the second component, the proximal cone tip, is diffraction-limited, the spread in the beam due to diffraction being much larger than the spread due to aberrations of the proximal tip, even for aperture diameters up to that of the largest cone tip (26 μm). As the cone-tip shape varies little between species, we can make this a general conclusion.

The structure of the first component, the corneal facet lens and distal crystalline cone, varies considerably from species to species (figures 8–12, 17–22); such a general conclusion about its aberrations is therefore not possible. Each type of corneal lens must be looked at individually to determine the quality and position of the intermediate image formed by it. We have shown above that the position of the intermediate image lies in the correct place, the waist region of the crystalline cone, to form an afocal system. The quality of the image can be examined directly by observing the images formed by the corneal lens, with a liquid of r.i. equal to that of the crystalline cone (1.48–1.50) behind the lens (see §5*b*). In many of the beetle species examined, the quality of this image was reasonable, implying that aberrations of the first component are not severe (§4*g*). However, a firm conclusion on this requires a more detailed investigation than we have yet been able to carry out. A second, complementary method of determining the quality of the image formed by the corneal lens is to measure the optical parameters of the lens and trace rays, as was done for the cone tip in §5*d*. This obviously shows only the image quality of a model corneal lens and is therefore much less satisfactory than direct observation, but does have the advantage of showing how sensitive the image quality is to the variations found in different facet lenses.

From our own observations on *Anoplognathus* and other species, the image formed by the corneal lens is quite distinct, indicating that the aberrations are not large; this is supported by the results from ray tracing through a model *Anoplognathus* corneal lens (that used in figure 7), which show that diffraction is probably the limiting factor here too. It would therefore appear that the aberrations of the two components are sufficiently small and the spacing of the components sufficiently accurate that diffraction at the pigment aperture at the proximal cone tip (the limiting aperture in an ommatidium) sets the size of the blur circle of light emerging from

PHILOSOPHICAL TRANSACTIONS OF THE ROYAL SOCIETY B BIOLOGICAL SCIENCES

each ommatidium. Pigment migration at this aperture therefore controls the optical performance of the individual ommatidia. The size of the blur circle is the diameter d_A of the Airy disc, or, in keeping with recent conventions in measuring angular acceptances, the width of the Airy disc at 50 % maximum intensity, equal to $0.42d_A$. Figure 26 shows the size of the blur circle in degrees and in micrometres at different distances behind the cone tip, for apertures of different diameter.

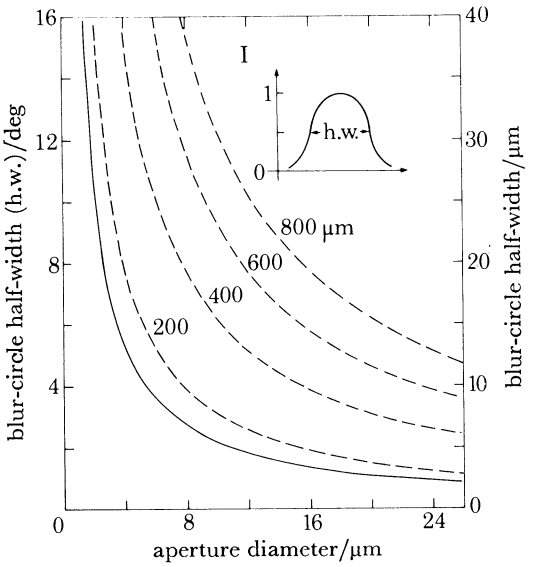

FIGURE 26. Diffraction effects at the crystalline-cone tip. The half-width (width at 50 % intensity) of the diffraction blur circle formed by light emerging from a cone tip, as a function of the diameter of the pigment aperture at the cone tip. The solid line shows the half-width in degrees subtended at the cone tip (left ordinate), and the dashed lines the half-width in micrometres (right ordinate) at four distances (200, 400, 600, 800 µm) behind the cone tip (right ordinate).

As an example, in *Anoplognathus* the rhabdoms lie about 340 µm behind the cones and each occupies an area approximately 15 µm in diameter (Meyer-Rochow & Horridge 1975). From figure 26 it can be seen that for apertures larger than about 8 µm, corresponding to the dark-adapted state, the blur circle (at the 50 % maximum level) will be smaller than the rhabdom. In the light-adapted state, the pigment aperture closes down to a diameter as small as 2 µm, thereby giving a blur circle much larger than the rhabdom. However, screening pigment that moves into the clear zone on light adaptation, partially or totally isolating the individual ommatidia (Meyer-Rochow & Horridge 1975), will absorb most of the spreading beam, leaving only a small amount on-axis to reach the rhabdom.

The blur circle resulting from diffraction is much larger than that due to aberrations of the cone tip (§5*d*). For example, the aberration blur circle at a distance of 350 µm behind the model cone of §5*d* is equivalent to that formed by diffraction at an aperture of 130 µm, rather than the 12 µm of the model. The system therefore has some tolerance to imperfections in either of the components or in the spacing of the components, i.e. the aberrations of the system can increase to a certain extent before the aberration blur circle becomes larger than the diffraction blur circle. This is of importance to the animal because there are likely to be errors or imperfections in r.i. gradients, cone dimensions, cornea–cone spacing, etc.

If the crystalline cone is not spaced correctly behind the cornea, the intermediate focus will

no longer lie in the waist region at the front focal point of the proximal crystalline cone. The resulting beam will then either diverge (intermediate focus too proximal) or converge and then diverge (intermediate focus too distal), and if the spacing is too much in error, the aberration blur circle will become larger than the diffraction blur cicle, resulting in a larger beam spread and a degradation of the image. We can determine the spacing tolerance of the system using our model of the proximal crystalline cone (§5*d*). The position of the intermediate focus is

Table 5. Spacing tolerance of the afocal system at different aperture diameters

aperture diameter/μm	tolerance/μm distally	tolerance/μm proximally
6	3	3
8	3	2.5
10	3	2
12	2.5	2
14	2.5	1.5
16	2.5	1.5
18	2	1.5
20	2	1.5
22	2	1.5
24	2	1.5
26	2	1.5

Tolerance values are given to the nearest ½ μm. Model parameters used are those of figure 25. The values given show the distance the intermediate image can deviate, distally or proximally, from the ideal (afocal) position without affecting the spread of the beam emerging from the cone tip. The aperture is the limiting aperture of the system, usually the pigment aperture at the proximal cone tip.

moved away from the ideal (afocal) position 23.6 μm distal to the tip, rays originating from this new position are traced through the cone tip and the size of the aberration blur circle determined at different distances behind the cone tip. The distance of the intermediate image from the ideal focus which gives an aberration blur circle equal in size to the diffraction blur circle determines the spacing tolerance of the system. This tolerance obviously depends on the diameter of the aperture at the cone tip, because this sets the size of the diffraction blur circle. Table 5 gives the spacing tolerance as a function of aperture diameter. In our model system, based on *Anoplognathus*, the tolerance is ± 2–3 μm over the range of apertures (6–12 μm) expected in the dark-adapted state, and this value does not decrease much even for the largest crystalline cones.

The first component of the afocal system has, by virtue of its restricted aperture (facet diameter), a depth of focus, i.e. the intermediate image formed by the first component is reasonable over several micrometres either side of best focus. In *Anoplognathus*, the value is about ± 4 μm. Provided that this range overlaps the range of tolerance of the second component, a reasonably collimated beam, with spread determined by diffraction, should emerge from the cone tip.

Diffraction-limited ommatidia are capable of projecting a beam equal in size to or smaller than a rhabdom, so that a superposition blur circle larger than a rhabdom is a result of incorrect aiming of the individual beams; this seems to us the more likely source of blurring of the superposition image, at least in scarab beetles. Even in a 'perfectly aligned' superposition eye, in which identical ommatidia are arranged around the circumference of a circle with their axes pointed towards the centre of the circle, there is a type of spherical aberration: the beams from

PHILOSOPHICAL TRANSACTIONS OF THE ROYAL SOCIETY B BIOLOGICAL SCIENCES

the more peripheral ommatidia are focused distal to those of the central ommatidia (Land *et al.* 1979). For a real eye even to approach this, the ommatidia must be aligned correctly and all have the same angular magnification. A detailed investigation of these factors in scarab eyes will be the subject of a future paper, but we can make several preliminary observations here.

The angular magnification M of an afocal system (the ratio of α/β: figure 1) is given by

$$M = f_1/f_2', \tag{13}$$

where f_1 is the front focal length of the first component and f_2' the back focal length of the second component; f_1 can be measured directly, as shown in §4*a*, while f_2' can be calculated from the ellipticity of the proximal cone tip and the r.i. of the centre and edge of the cone and of the surrounding clear zone, i.e. by indirect observation. (If the r.i. gradient remains approximately the same from cone to cone in a given species, f_2' can be found from a simple measurement of tip ellipticity.) The angular magnification can then be found quite rapidly for a number of neighbouring ommatidia. The value of M is not sensitive to incorrect spacing of the cornea and cone, so that, if the intermediate image does not fall exactly in the right position, the beam will still emerge at the angle given by equation (13) for an afocal system, but will be more spread as discussed above.

For the superposition image to be formed at the distal rhabdom tips, the angular magnification must be matched to the clear-zone width. If the cone tips lie on the circumference of a circle of radius R_1 (with the ommatidial axes pointing towards the centre) and the distal rhabdom tips on a concentric circle of radius R_2 (see figure 28), the relation (Exner 1891; Diesendorf & Horridge 1973; Land *et al.* 1979)

$$M = \frac{R_2}{R_1 - R_2} \tag{14}$$

must hold. The matching of the ommatidial optics to the clear zone can therefore be determined by measurement, on the one hand, of M from the focal lengths of the two components (equation 13) and, on the other hand, of R_1, R_2.

It is possible to design a 'perfect' superposition eye in which all beams superimpose exactly, by adopting a slightly different geometry (Land *et al.* 1979). However, this eye functions perfectly only for one direction and has a limited field of view, making it unsuitable as an 'all-round' eye. Whether this type of structure occurs in scarab eyes remains to be seen.

The ultimate test of the hypotheses in this paper is of course the actual size of the superposition image in an intact eye. This, too, remains to be determined for almost all scarab beetles (but see Meyer-Rochow & Horridge 1975), by either optical, electrophysiological or behavioural techniques (review, Horridge 1975). Note that these techniques, with the possible exception of the first, only determine how well the dioptric system works and not how it works.

(*b*) *Why graded-refractive-index lenses?*

We have already seen in §4 that beetles with thick corneas cannot use a front-surface curvature on the facet lens to focus light, because, with even a slight curvature, the intermediate focus would lie within the cornea rather than in the crystalline cone. (For different reasons corneal lenses in aquatic beetles and nocturnal beetles also do not have a front-surface curvature.) The refracting power of the corneal lens is provided instead by an internal g.r.i. lens located in the proximal region of the corneal facet, allowing the intermediate image to fall in the correct

place. A curved back surface to the cornea alone would provide insufficient refracting power, because the r.i. drop across it is not large.

A more compelling reason for g.r.i. lenses can be seen by examining alternatives to the g.r.i. lens in the proximal cone tip. Is it possible to design, say, a homogeneous cone tip with similar focusing properties to those of the g.r.i. lens (figure 25)? A homogeneous hemiellipsoid (an

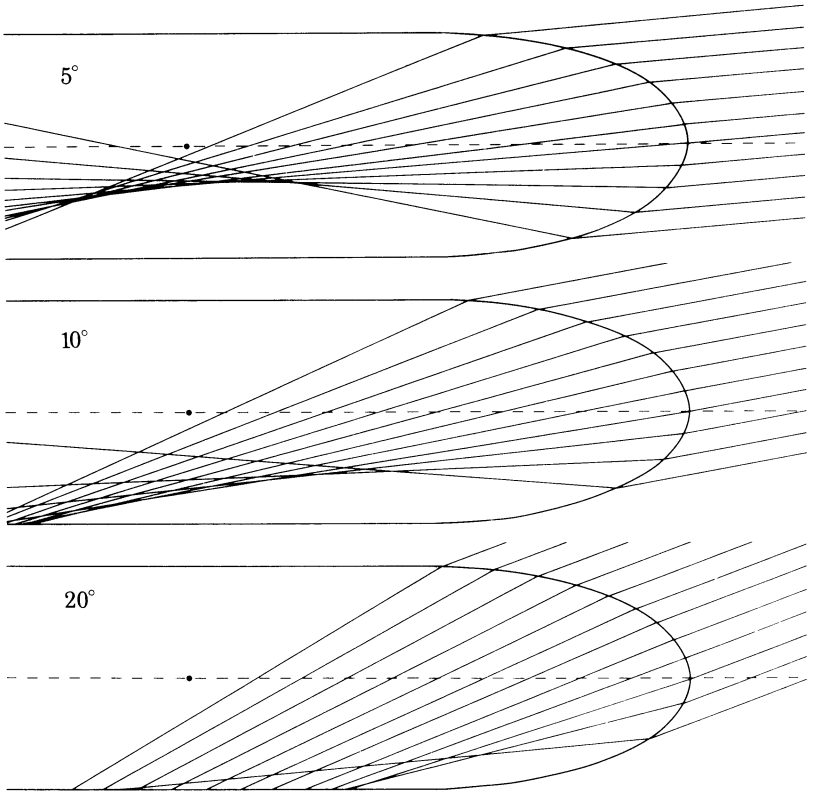

FIGURE 27. Ray tracing through a homogeneous elliptical cone at various angles of incidence. The r.i. inside the ellipse is 1.48, outside 1.34, and the ellipticity $y_b/x_b = 0.425$ is chosen to give a point focus for on-axis (0°) light (marked by •) at a distance of 23.6 μm from the cone tip, the same distance as found from the model g.r.i. lens.

ellipsoidal surface with homogeneous media on either side, that with the higher r.i. lying inside) has the property that, if the ellipticity is matched to the r.i. difference across the surface (Levi 1968), a parallel beam incident at 0° is brought to a point focus (assuming no diffraction). However, as shown in figure 27, the focus for beams at an angle to the axis deteriorates rapidly as the angle increases, and by 20° the focus is very poor and, such as it exists, no longer within the cone. A homogeneous hemiellipsoid is therefore unsuitable as the second component of the afocal system, which must operate well at angles up to about 20°. A homogeneous hemisphere fares even worse, suffering from bad spherical aberration (0°) as well. A g.r.i. lens appears essential for the proximal cone tip to function as required. Note that the homogeneous hemiellipse, which is constructed to have the same distance from tip to focus as the g.r.i. hemiellipse, has about the same ellipticity; the g.r.i. properties act to 'tidy up' the off-axis rays, ensuring they come approximately to a point focus.

Given that the cone tips are almost always hemiellipsoidal, it is interesting to find that a model hemispheric g.r.i. lens (plus g.r.i. lens cylinder) performs as well as the hemiellipsoidal

g.r.i. lens (plus g.r.i. lens cylinder), for beams (meridional rays only) incident at angles up to at least 20°, as in figure 25. It is possible that a hemiellipsoidal shape focuses skew rays more accurately than does a hemispherical shape, but to test this requires a three-dimensional ray trace through the proximal cone tip, a project that we have not yet undertaken. An ellipsoidal tip to the crystalline cone may also allow finer control of the aperture size by mobile screening pigment.

(*c*) *Physiological ecology in lens design*

Winged beetles always have well developed compound eyes, whereas the eyes of flightless species are often reduced (Jeannel 1965). For example, the eyes of flightless canthonine dung beetles of Australian forests are small in comparison with those of allied flying species (Matthews 1974). Clearly the eye has an important role in flight; it not only serves in flight navigation, but may also control the timing of flight initiation by monitoring ambient light levels (Lewis & Taylor 1965). Another general rule is that the eyes of day-flying lamellicorns are smaller than those of their crepuscular and nocturnal relatives of similar body size (a notable exception is the diurnal cetoniines, which have large eyes).

Most lamellicorns forage on the wing, although the extent to which the eyes are used to locate food varies considerably. While the diurnal chafers (Cetoniinae) possess high visual acuity in seeking flowers (H. Howden, personal communication), dung beetles are not as dependent on visual cues to detect food (Halffter & Matthews 1966), rather they fly upwind and locate dung with antennal chemoreceptors (although there appears to be some visual location when near the dung pad). During flight, the eye of the dung beetle serves primarily to avoid obstacles. One might predict differences in lens design in the compound eyes of different scarab species, since flight activity in most species is confined to a very limited period of the day. Three main patterns of activity are seen: *diurnal* (flight in the hours of daylight, mainly morning through to early afternoon); *crepuscular* (flight at dusk and, to a lesser extent, at dawn); and *nocturnal* (flying during the hours of darkness). Although the basis for these patterns of activity is no doubt complex, if we assume that dung beetles fly mainly to colonize new dung resources, a possible explanation for this striking periodicity in flight activity is available. Consider, for example, the African dung beetles. On the plains of east Africa, the fresh dung of the large mammals is a highly attractive but transient commodity (Heinrich & Bartholomew 1979). Its production fluctuates during the day, being greatest at dawn and dusk, and around midday. The intense competition for dung may be the reason why different species of ball-rolling dung beetles have flight patterns coinciding with one (or more) of these periods (Tribe 1976; Heinrich & Bartholomew 1979). Many crepuscular endocoprid species (such as *Onitis alexis* and *Onthophagus gazella*) fly briefly during a 30 min period at dusk (K. Houston, personal communication). The giant dung beetle *Heliocopris dilloni* flies to fresh dung at night (Kingston & Coe 1977). The tribe Oniticellini (*Oniticellus* spp., *Euoniticellus* spp.) and members of the genus *Phanaeus* (Fincher *et al.* 1971) fly mainly in the day. Although whole subfamilies in the Scarabaeidae can be classed as diurnal (e.g. Cetoniinae) or crepuscular–nocturnal (e.g. Dynastinae, Melolonthinae) we were particularly interested in examining the eyes of closely related species, preferably in the same genus, that display extremes in daily activity pattern. The Scarabaeinae (dung beetles) were an obvious choice to study ecological adaptation in the eucone clear-zone eye, in that conspecifics in many genera can be classified as diurnal, crepuscular or nocturnal in activity (table 3).

PHILOSOPHICAL TRANSACTIONS OF THE ROYAL SOCIETY B BIOLOGICAL SCIENCES

Although there are differences in relative eye size in diurnal and nocturnal dung beetle species (Matthews 1972), it is at the level of the individual corneal facet and crystalline cone that dramatic differences in lens design in species of differing diel activity are evident. Fixed screening pigment in the cornea is seen almost exclusively in day-flying species, where it lines the corneal lens cylinders to varying extents (table 3). Similar corneal screening pigment has been reported in diurnal moths and tiger beetles (Friederichs 1931). In the lamellicorns its distribution appears to be restricted to diurnal stag beetles (e.g. *Lamprima*) and to diurnal members of the two most advanced scarabaeid subfamilies, the dung beetles and the flower chafers. Corneal screening pigment is especially well developed in the African members of the ball-roller genera *Kheper* and *Scarabaeus* that are diurnal in activity, presumably to protect the ommatidia from the blinding glare of the African sun. The presence of pigment in the distal corneal region is always associated with a strong front facet curvature. Nocturnal conspecifics have glacial corneas with no corneal pigment. This relationship holds true for several tribes of the Scarabaeinae (table 3). The sacred scarab, *Scarabaeus sacer*, is a notable exception to this general pattern. According to folklore, it rolls dung balls during the daytime, but we could find no record of its flight activity pattern.† *Geotrupes spiniger*, too, does not fit the pattern. Although *G. spiniger* is predominantly crepuscular, most species of this genus will forage in the daytime (*Geotrupes stercorarius* flies in hot sunshine (Rye 1866)) which might explain the corneal screening pigment and strong facet curvature seen in all species of this genus examined. In broad terms, then, there are distinct differences in corneal anatomy in diurnal and nocturnal dung beetles. But can slight differences in corneal design be used to predict subtle variations in flight activity? Consider the tribe Onitini. Although species of *Chironitis* fly around midday (e.g. *C. scabrosus*; A. Davis, personal communication), most species of *Onitis* are crepuscular and/or nocturnal. Yet three species of about the same size, *O. alexis*, *O. aygulus* and *O. deceptor*, have quite distinct corneal anatomy (table 3). *O. alexis* has a slight deposit of corneal pigment and individual front facet curvature, *O. aygulus* has facet curvature only, while *O. deceptor* has neither feature. Although flight records for these species are incomplete, preliminary data suggest that the dusk flight of *O. alexis* is, on average, slightly earlier than that of *O. deceptor* (P. Stickler, C.S.I.R.O. internal report). No information is available for *O. aygulus*, except that it is crepuscular in flight activity. The related species *Bubas bubaloides* is seen on the wing during the day as well as at dusk (K. Paschalidis, personal communication) and, like *Chironitis*, has corneal screening pigment.

Corneal facet anatomy in those scarabs with exocone clear-zone eyes is far less variable, possibly because of their fairly uniform (crepuscular–nocturnal) flight activity. However, the eye of the rather atypical day-flier, the bolboceratine *Stenaspidius*, has very narrow facets and strongly tapered and waisted exocones (table 2). Nocturnal species have little taper to their large exocones, although in *Aulacocyclus* a waist is present. Unlike for beetles of similar habits with eucone eyes, screening pigment is absent from the *Stenaspidius* cornea. A reduction in corneal facet diameter in diurnal scarabs is a commonly seen strategy where resolution rather than absolute sensitivity to light is the major consideration.

Similarly, the crystalline cone in the scarab eucone eye shows considerable variation in form that can be related to the activity pattern of the beetle concerned. In nocturnal beetles, the

† Paulian (1959) asserts that Fabre's classic description of the natural history of the sacred scarab was based on observations of *Scarabaeus affinis*, not *S. sacer*. Paulian states that, although *S. affinis* is active in the morning and buries its dung ball in the afternoon, it is attracted to u.v. light at night. A similar activity pattern in *S. sacer* would explain its corneal structure.

PHILOSOPHICAL TRANSACTIONS OF THE ROYAL SOCIETY B BIOLOGICAL SCIENCES

crystalline cone is typically large, with a wide angular acceptance and a broad ellipsoidal tip. We regard this to be the ancestral shape, as the evolutionary prototype of the modern scarab very probably flew at low light intensities (Crowson 1960). As certain scarab groups became more diurnal in habit, several alternative strategies in lens design in the eye have been adopted. Many scarabs, for instance the diurnal dung beetles (*Euoniticellis africanus*: Meyer-Rochow 1978), have evolved a *diurnal superposition eye* in which the aperture formed by the screening pigment around the crystalline cone tip remains open, and a crystalline tract is not developed, at high light intensities. (A similar strategy has been adopted by some day-flying moths (Horridge *et al.* 1977).) In these scarabs, although superposition optics have been retained for daytime use, the angular acceptance of the individual facets has been reduced by the development of a strong waist at the intermediate focal plane (best exemplified by diurnal species of *Scarabaeus*) or by the presence of a taper in the bullet-shaped cone (as in *Euoniticellus*). In both instances, the maximum effective aperture for superposition image formation is reduced (figure 28). Both cone shapes described here would reduce the light flux onto the rhabdom. Provided that the exit aperture at the crystalline cone tip remained greater than say, 10 μm, diffraction effects would not be detrimental to image formation. A second strategy adopted by other diurnal beetles appears to be a more extreme evolutionary solution. Whereas many crepuscular and nocturnal scarabs (e.g. *Anoplognathus*: Meyer-Rochow & Horridge 1975) have clear-zone superposition eyes that, at high light intensities, become apposition eyes by the migration of screening pigment to the proximal cone tip and the development of a pigment-lined crystalline tract, many diurnal scarabs have evolved an eye that is, to all intents and purposes, a *permanent clear-zone apposition eye*. The strongly tapered crystalline cone (as seen by other authors in the Cetoniinae) and the greatly reduced cones of *Phyllopertha* and *Lamprima* would be less able to project a good superposition image across the clear zone. Perhaps this is why these cone shapes are restricted to scarabs active in sunshine, many of whom will not fly in dull weather.

Finally, it should be noted that Kuster (1979) has reported considerably anatomical differences in the compound eyes of diurnal and crepuscular cicindelid and carabid beetles. While crepuscular species have a well developed clear zone, it is much reduced in width in diurnal species. Several diurnal dung beetles have reduced clear zones, particularly in the dorsal region of the eye (S. C., unpublished observations).

(*d*) *Lens design in relation to scarab phylogeny*

The lamellicorns form one of the most sharply defined sections of the Coleoptera. Although there is virtually no difference of opinion as to the families that compose the group (Crowson 1955), the relationship between the families in the group (as well as the relationship of the lamellicorns to other beetle groups) is obscure. In evolutionary terms, the lamellicorns are among the most advanced of the Coleoptera, appearing alongside the flowering plants in the Cretaceous (Moore 1978). The passalids, followed closely by the lucanids, with their simple wood-feeding larval habits, would have been among the first to evolve (Moore 1978). At the other end of the evolutionary scale, the two main branches of the true scarab family (Scarabaeidae), the coprophagous laparasticts and the phytophagous pleurosticts, culminate in the highly advanced dung beetles (Scarabaeinae) and flower chafers (Cetoniinae) respectively. The position of the carrion-feeding trogids and the predominantly mycetophagous geotrupids in this evolutionary scheme is unclear. Although the development of an ocular canthus has been used frequently as a diagnostic feature to distinguish scarabs at the subfamily and generic

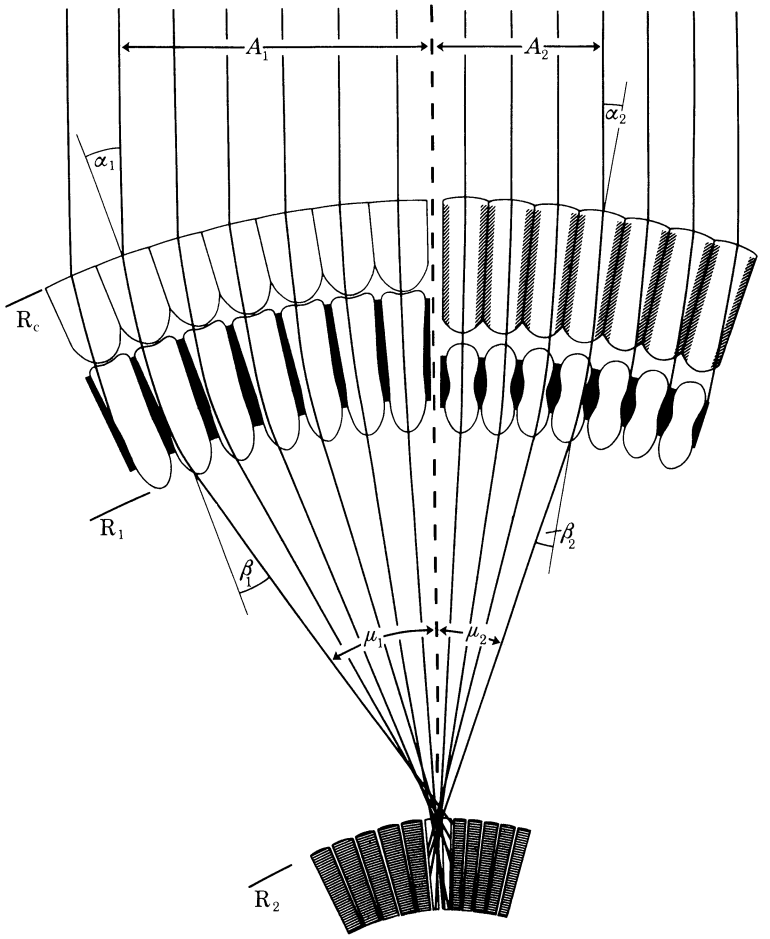

FIGURE 28. Summary diagram of differences in optical design of the superposition eye in nocturnal and diurnal beetles. The effective aperture of the superposition eye is set by the number of facets (more strictly, the area of eye surface) capable of capturing incident light from a distant point source and focusing it onto the rhabdom layer to form a superposition image. This effective aperture is greatest in nocturnal beetles ($2A_1$, left). Here rays striking the eye surface at angles up to α_1 are focused by the lens elements into a cone of light subtending an angle of $2\mu_1$ (the aperture angle) at the distal rhabdom level. The waist region of the crystalline cone sets the maximum effective aperture. Although diurnal beetles may use superposition optics, the number of facets that contribute to form an image of a similar object may be considerably less (right). This is because the pigment (solid black) associated with the stronger waist in the crystalline cone of diurnal beetles acts as a field stop and eliminates light rays that strike the eye surface at angles greater than α_2 ($<\alpha_1$). By reducing the angular acceptance of the individual ommatidia, the waist limits the maximum effective aperture to $2A_2$ and consequently the angle subtended by the cone of light focused on the rhabdom layer ($2\mu_2$). The corneal screening pigment (diagonal cross-hatching) prevents light crossing between ommatidia, thus further limiting the light flux across the clear zone and helping to eliminate stray light. Both optical systems show the proximal tip of the crystalline cone with the exit pupil wide open, i.e. the proximal pigment fully retracted, as seen in the dark-adapted state. Reduction of this aperture-stop diameter in bright light would reduce light flux across the clear zone, but not the number of facets forming the superposition image; this is reduced by the screening pigment moving into the clear zone to optically isolate the individual ommatidia (see text). When the pigment is in the fully retracted state, the diffraction blur circle of a single ommatidium can have a diameter as small as that of a single rhabdom. The diameter of the superposition blur circle depends on the alignment of the contributing ommatidia. The ratio of the entrance angle α and the exit angle β is the angular magnification (M) of the system. In both the nocturnal and diurnal superposition eyes shown here, $M = 1$.

PHILOSOPHICAL TRANSACTIONS OF THE ROYAL SOCIETY B BIOLOGICAL SCIENCES

levels (Lucanidae (Holloway 1969), Geotrupidae (Portevin 1931)), this paper describes finer aspects of corneal anatomy that may be of broader phylogenetic significance.

In spite of considerable difference in body appearance, the passalids, together with the bolboceratine and pleocomine geotrupids, have well developed exocone projections in the cornea. In the other scarab families and geotrupid subfamilies a crystalline cone is found instead. In spite of their biochemical and developmental differences, the exocone and crystalline cone have similar g.r.i. lens properties and presumably similar function in the clear-zone eye. We suggest that, once one or the other optical system had been selected during evolution, there would be little pressure to turn to the other. Consequently, this dichotomy in the fundamental design of the lens system in the compound eye, in contrast to the more subtle modifications seen when the eyes of diurnal and nocturnal species are compared, may be a useful indicator of phylogenetic relationships within the Scarabaeoid superfamily.

Beetles with exocone clear-zone eyes appear to be relatively primitive; not only are they virtually all nocturnal in habit, but the ventral nervous system in their larvae displays the least condensation of the abdominal ganglia (*Popilius disjunctus* (Passalidae) (Cody & Gray 1938); *Pleocoma crinita* (Pleocominae) (Areekul 1957)).

(*e*) *Final comments*

Our basic assumption was that the scarab compound eye functions according to Exner's superposition principle, in which g.r.i. lenses are involved. As we set out to test if the dioptric elements, by virtue of their optical properties, were compatible with Exner's principle, further subtleties in lens design became evident that gave it extra support. G.r.i. lenses are not easy to make; only very few g.r.i. lenses with curved surfaces have been manufactured. The regularity in form, the precise near-parabolic internal gradients in r.i., suggest to us that in dung beetles, at least, an afocal, relatively aberration-free, g.r.i. optical system (within the constraints of lens size) has evolved. The variation in maximum angular acceptance at the primary focal plane, as demarcated by the waist in the crystalline cone, supports the notion that superposition optics are used by members of this group over a wide range of light intensities. Superposition optics is not an option available exclusively to crepuscular/nocturnal species. Optical quality is safe-guarded during lens development in the ommatidium by an inherently precise mechanism, the abutment of cornea and crystalline cone, which ensures the correct alignment of dioptric elements, together with an insensitivity to scaling and a certain tolerance to spacing of the lens elements. The optical properties of the clear zone and the optical geometry of the scarab eye as a whole remain to be studied. We would predict that permanent or light-inducible crystalline tracts are present in the eyes of many day-active species. By extending into the clear zone, crystalline tracts would downgrade the quality of the superposition image, but whether this has important visual consequences in these beetles is unclear. A poorly focused superposition image (as seen in crepuscular chafer eyes) probably results from allowing a large number of facets to contribute to the superposition image. This gives a high absolute sensitivity, but, because of alignment inaccuracies associated with a large number of facets, the resolution suffers. In these eyes, dioptric quality, in theory and in practice, is not as crucial.

This paper would not have seen the light of day had it not been for the assistance of many people. Professor Adrian Horridge kindly provided space and facilities to undertake this research, while Dr Murray Wallace of the Dung Beetle Research Project in the Division of

PHILOSOPHICAL TRANSACTIONS OF THE ROYAL SOCIETY B BIOLOGICAL SCIENCES

Entomology, C.S.I.R.O., allowed us to tap the resources of his research group. We are particularly grateful to Dr Keith Houston and Dr Barry Moore of the C.S.I.R.O. as well as Dr Henry Howden in Ottawa, for their advice and encouragement relating to beetle biology, and to Dr Colin Pask and Melanie Campbell (Applied Mathematics, Australian National University (A.N.U.)) for mathematical advice.

Beetle material came from many sources: Bruce Ham (A.N.U.) and Dr Vance Brown (C.S.I.R.O.) trapped live *Anoplognathus*; Noel Starrick, Peter Hart and John Feehan (C.S.I.R.O.) provided laboratory-reared dung beetles; Eric Holm (C.S.I.R.O.) supplied alcohol-fixed dung beetles; Mick Bacchus (British Museum (Natural History)) supplied pickled chafers; Barry Moore supplied several stag beetles; and Henry Howden sent us geotrupines and bolboceratines. The passalid we actually caught ourselves. Tom Wier, John Lawrence (C.S.I.R.O.) and Adrian Davis (Pretoria) assisted in our identification of several species. We thank them all.

The diagrams were proficiently drawn by Garry Brown (A.N.U.). Kerrie Ruth (A.N.U.) and Ian Craig (University of Western Ontario) provided patient photographic assistance.

The Natural Sciences and Engineering Research Council of Canada provided financial support in the form of a sabbatical travel grant to S.C.

References

Areekul, S. 1957 The comparative internal larval anatomy of several genera of Scarabaeidae (Coleoptera). *Ann. ent. Soc. Am.* **50**, 562–577.

Blest, A. D. & Land, M. F. 1977 The physiological optics of *Dinopis subrufus* L. Koch: a fish-eye lens in a spider. *Proc. R. Soc. Lond.* B **196**, 197–222.

Buddenbrock, W. von 1952 Vergleichende Physiologie. *Sinnesphysiologie*, vol. 1. Basel: Birkhäuser.

Bugnion, E. & Popoff, N. 1914 Les yeux des insectes nocturnes. *Archs Anat. microsc.* **16**, 289–304.

Cleary, P., Deichsel, G. & Kunze, P. 1977 The superposition image in the eye of *Ephestia kühniella*. *J. comp. Physiol.* **119**, 73–84.

Cody, F. P. & Gray, I. E. 1938 The changes in the central nervous system during the life history of the beetle, *Passalus cornutus* Fabricius. *J. Morph.* **62**, 503–521.

Crowson, R. A. 1955 *The natural classification of the families of* Coleoptera. London: Nathaniel Lloyd.

Crowson, R. A. 1960 The phylogeny of Coleoptera. *A. Rev. Ent.* **5**, 111–134.

Diesendorf, M. & Horridge, G. A. 1973 Two models of the partially focused clear-zone compound eye. *Proc. R. Soc. Lond.* B **183**, 141–158.

Exner, S. 1876 Über das Sehen von Bewegungen und die Theorie des zusammengesetzten Auges. *Sber. Akad. Wiss. Wien* (*math.-nat. Kl.*) **72**, 157–191.

Exner, S. 1885 Ein Micro-Refraktometer. *Arch. mikrosk. Anat. EntwMech.* **25**, 97–112.

Exner, S. 1891 *Die Physiologie der facettirten Augen von Krebsen und Insecten*. Leipzig and Vienna: Franz Deuticke.

Fincher, G. T., Davis, R. & Stewart, T. B. 1971 Flight activity of coprophagous beetles on a swine pasture. *Ann. ent. Soc. Am.* **64**, 855–860.

Fletcher, A., Murphy, T. & Young, A. 1954 Solutions of two optical problems. *Proc. R. Soc. Lond.* A **223**, 216–225.

Friederichs, H. F. 1931 Beiträge zur Morphologie und Physiologie der Sehorgane der Cicindelinen (Col.). *Z. Morph. Ökol. Tiere* **21**, 1–172.

Galbraith, W. 1955 The optical measurement of depth. *Q. Jl microsc. Sci.* **96**, 285–288.

Grenacher, H. 1879 *Untersuchungen über das Sehorgan der Arthropoden insbesondere der Spinnen, Insekten und Crustaceen*. Göttingen: Vandenhock and Ruprecht.

Halffter, G. & Matthews, E. D. 1966 The natural history of dung beetles of the subfamily Scarabaeinae (Coleoptera, Scarabaeidae). *Folia ent. mex.*, nos. 12–14.

Hausen, K. 1973 Die Brechungsindices im Kristallkegel der Mehlmotte *Ephestia kühniella*. *J. comp. Physiol.* **82**, 365–378.

Heinrich, B. & Bartholomew, G. A. 1979 Roles of endothermy and size in inter- and intraspecific competition for elephant dung in an African dung beetle, *Scarabaeus laevistriatus*. *Physiol. Zool.* **52**, 484–496.

Holloway, B. 1969 Further studies on generic relationships in the Lucanidae (Insecta: Coleoptera) with special reference to the ocular canthus. *N. Z. Jl Sci.* **12**, 958–977.

Horridge, G. A. 1975 Optical mechanisms of clear-zone eyes. In *The compound eye and vision of insects* (ed. G. A. Horridge), pp. 255–298. Oxford: Clarendon Press.

PHILOSOPHICAL TRANSACTIONS OF THE ROYAL SOCIETY B BIOLOGICAL SCIENCES

Horridge, G. A. 1976 Arthropod receptor optics. In *Photoreceptor optics* (ed. A. W. Snyder & R. Menzel), pp. 459–478. Berlin: Springer-Verlag.
Horridge, G. A. & Giddings, C. 1971 Movement on dark and light-adaptation in beetle eyes of the neuropteran type. *Proc. R. Soc. Lond.* B **179**, 73–85.
Horridge, G. A., Giddings, C. & Stange, G. 1972 The superposition eye of skipper butterflies. *Proc. R. Soc. Lond.* B **182**, 457–495.
Horridge, G. A., McLean, M., Stange, G. & Lillywhite, P. G. 1977 A diurnal moth superposition eye with high resolution *Phalaenoides tristifica* (Agaristidae). *Proc. R. Soc. Lond.* B **196**, 233–250.
Jeannel, R. 1965 Ordre des Coléoptères. In *Traité de zoologie*, vol. 9 (ed. P.-P. Grassé), pp. 771–1117. Paris: Masson.
Kapron, F. P. 1970 Geometrical optics of parabolic index-gradient cylindrical lenses. *J. opt. Soc. Am.* **60**, 1433–1436.
Kingston, T. J. & Coe, M. 1977 The biology of a giant dung beetle (*Heliocopris dilloni*). *J. Zool.* **181**, 243–263.
Kirchhoffer, O. 1908 Untersuchungen über die Augen pentamerer Käfer. *Arch. Biontol.* **2**, 235–287.
Kunze, P. 1979 Apposition and superposition eyes. In Vision in invertebrates, *Handbook of sensory physiology*, vol. 7, pt 6A (ed. H. Autrum), pp. 441–502. Berlin: Springer-Verlag.
Kuster, J. E. 1979 Comparative structure of compound eyes of Cicindelidae and Carabidae (Coleoptera): Evolution of scotopy and photopy. *Quaest. ent.* **15**, 297–334.
Land, M. F. 1980*a* Optics and vision in invertebrates. In Vision in invertebrates, *Handbook of sensory physiology*, vol. 7, pt 6B (ed. H. Autrum), pp. 471–592. Berlin: Springer-Verlag.
Land, M. F. 1980*b* Compound eyes: old and new optical mechanisms. *Nature, Lond.* **287**, 681–685.
Land, M. F., Burton, F. A. & Meyer-Rochow, V. B. 1979 The optical geometry of euphausiid eyes. *J. comp. Physiol.* **130**, 46–62.
Levi, L. 1968 *Applied optics. A guide to optical system design*, vol. 1. New York: Wiley.
Lewis, T. & Taylor, L. R. 1965 Diurnal periodicity of flight by insects. *Trans. R. ent. Soc. Lond.* **116**, 393–479.
Longhurst, R. S. 1973 *Geometrical and physical optics* (3rd edn). London: Longmans, Green.
Luneburg, R. K. 1964 *Mathematical theory of optics*. Berkeley: University of California Press.
Marchand, E. W. 1978 *Gradient index optics*. New York: Academic Press.
Matthews, E. G. 1972 A revision of the scarabaeine dung beetles of Australia. I. Tribe Onthophagini. *Aust. J. Zool., Suppl. Ser.*, no. 9.
Matthews, E. G. 1974 A revision of the scarabaeine dung beetles of Australia. II. Tribe Scarabaeini. *Aust. J. Zool., Suppl. Ser.*, no. 24.
Meggitt, S. & Meyer-Rochow, V. B. 1975 Two calculations on optically non-homogeneous lenses. In *The compound eye and vision of insects* (ed. G. A. Horridge), pp. 314–320. Oxford: Clarendon Press.
Meyer-Rochow, V. B. 1973 The dioptric system of the eye of *Cybister* (Dytiscidae: Coleoptera). *Proc. R. Soc. Lond.* B **183**, 159–178.
Meyer-Rochow, V. B. 1975 The dioptric system in beetle compound eyes. In *The compound eye and vision of insects* (ed. G. A. Horridge), pp. 299–313. Oxford: Clarendon Press.
Meyer-Rochow, V. B. 1977 Structure and possible function of the unusual compound eye of *Sericesthis geminata* (Coleoptera: Scarabaeidae). *N. Z. Jl Zool.* **4**, 21–34.
Meyer-Rochow, V. B. 1978 Retina and dioptric apparatus of the dung beetle *Euoniticellus africanus*. *J. Insect Physiol.* **24**, 165–179.
Meyer-Rochow, V. B. & Horridge, G. A. 1975 The eye of *Anoplognathus* (Coleoptera, Scarabaeidae). *Proc. R. Soc. Lond.* B **188**, 1–30.
Moore, B. P. 1978 A new Australian stag beetle (Coleoptera: Lucanidae) with neotropical affinities. *J. Aust. ent. Soc.* **17**, 99–103.
Paulian, R. 1959 Coléoptères scarabéides (2nd edn). *Faune Fr.* **63**.
Portevin, G. 1931 *Histoire naturelle des Coléoptères de France*, vol. 2. Paris: Lechevalier.
Ross, K. F. A. 1967 *Phase contrast and interference microscopy for cell biologists*. London: Arnold.
Rye, E. C. 1866 *British beetles*. London: Reeve.
Sands, P. J. 1971 Inhomogeneous lenses. III. Paraxial optics. *J. opt. Soc. Am.* **61**, 879–885.
Schultze, M. 1868 *Untersuchungen über die zusammengesetzen Augen der Krebse und Insekten*, pp. 1–32. Anat. Inst. Bonn.
Seitz, G. 1969 Untersuchungen am dioptrischen Apparat des Leuchkäferauges. *Z. vergl. Physiol.* **62**, 61–74.
Tribe, G. D. 1976 *The ecology and ethology of ball-rolling dung beetles* (Coleoptera: Scarabeidae). M.Sc. thesis, University of Natal.
Vogt, K. 1974 Optische Untersuchungen an der Cornea der Mehlmotte *Ephestia kühniella*. *J. comp. Physiol.* **88**, 201–216.

PHILOSOPHICAL TRANSACTIONS OF THE ROYAL SOCIETY B BIOLOGICAL SCIENCES

PHILOSOPHICAL TRANSACTIONS OF THE ROYAL SOCIETY B BIOLOGICAL SCIENCES

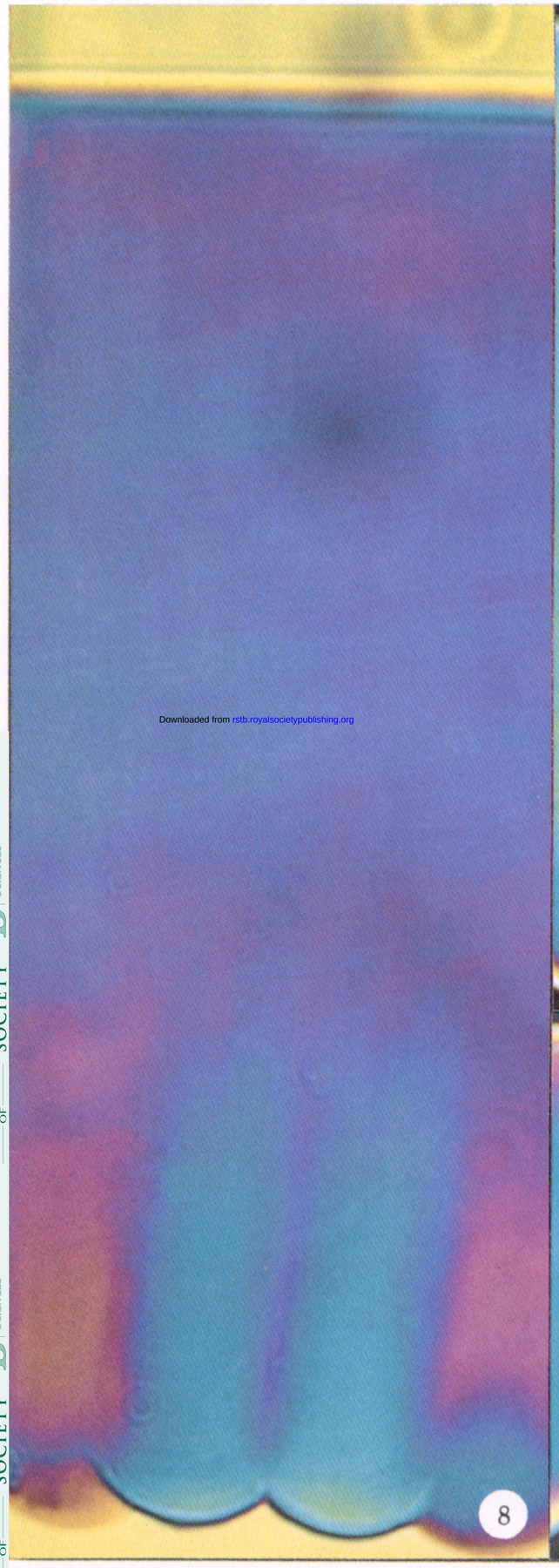

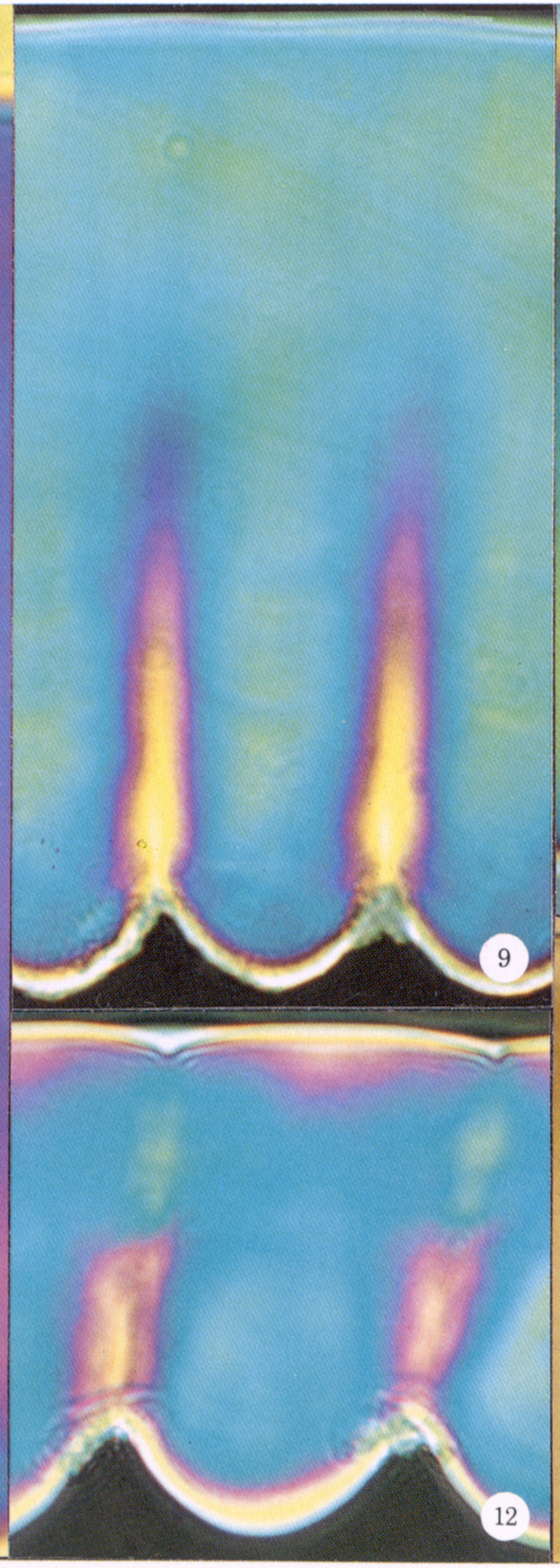

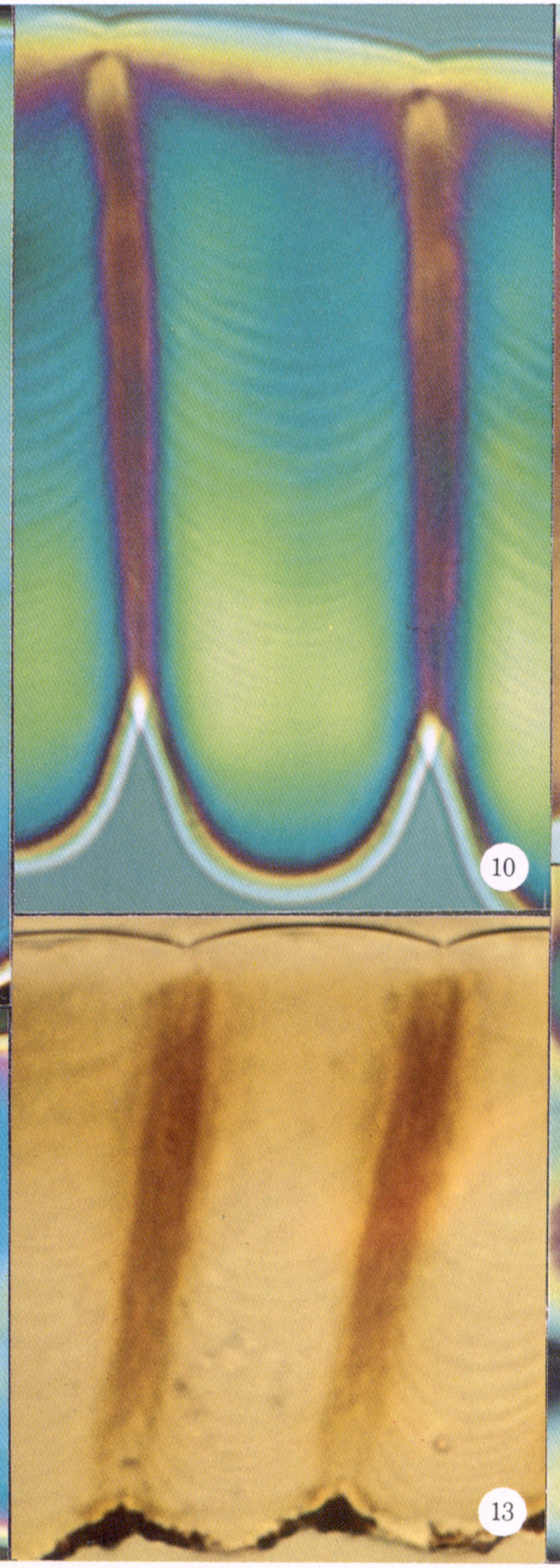

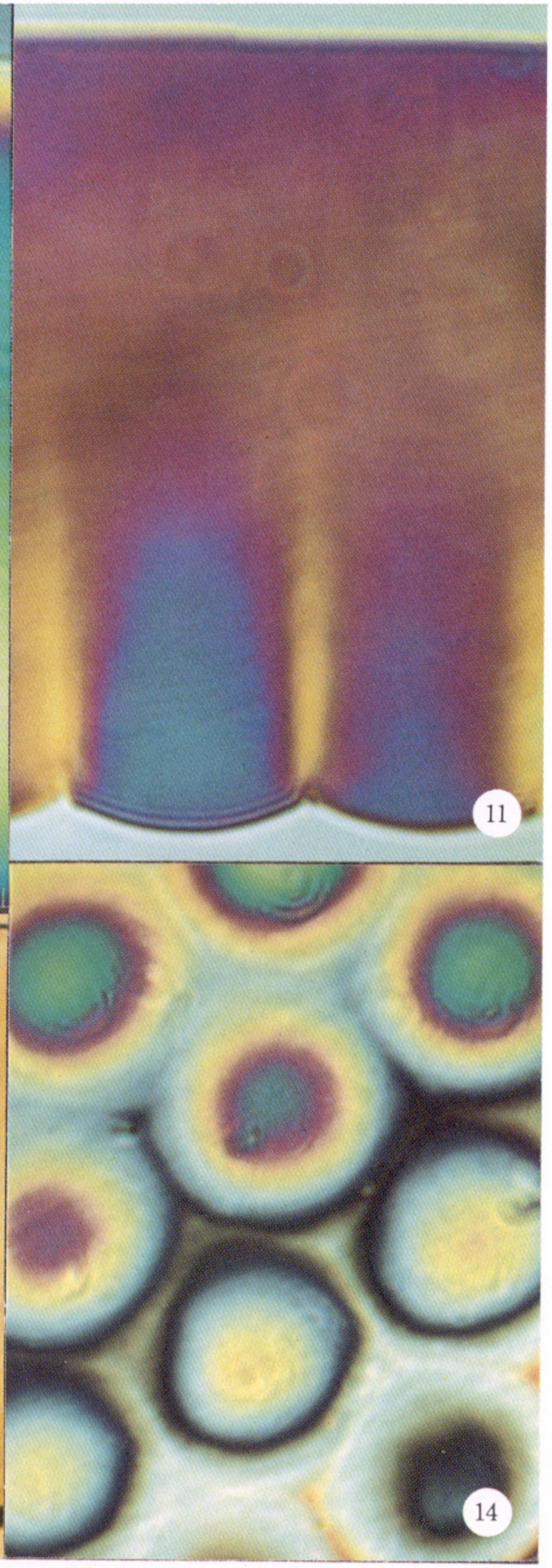

FIGURES 8–14. For description see opposite.

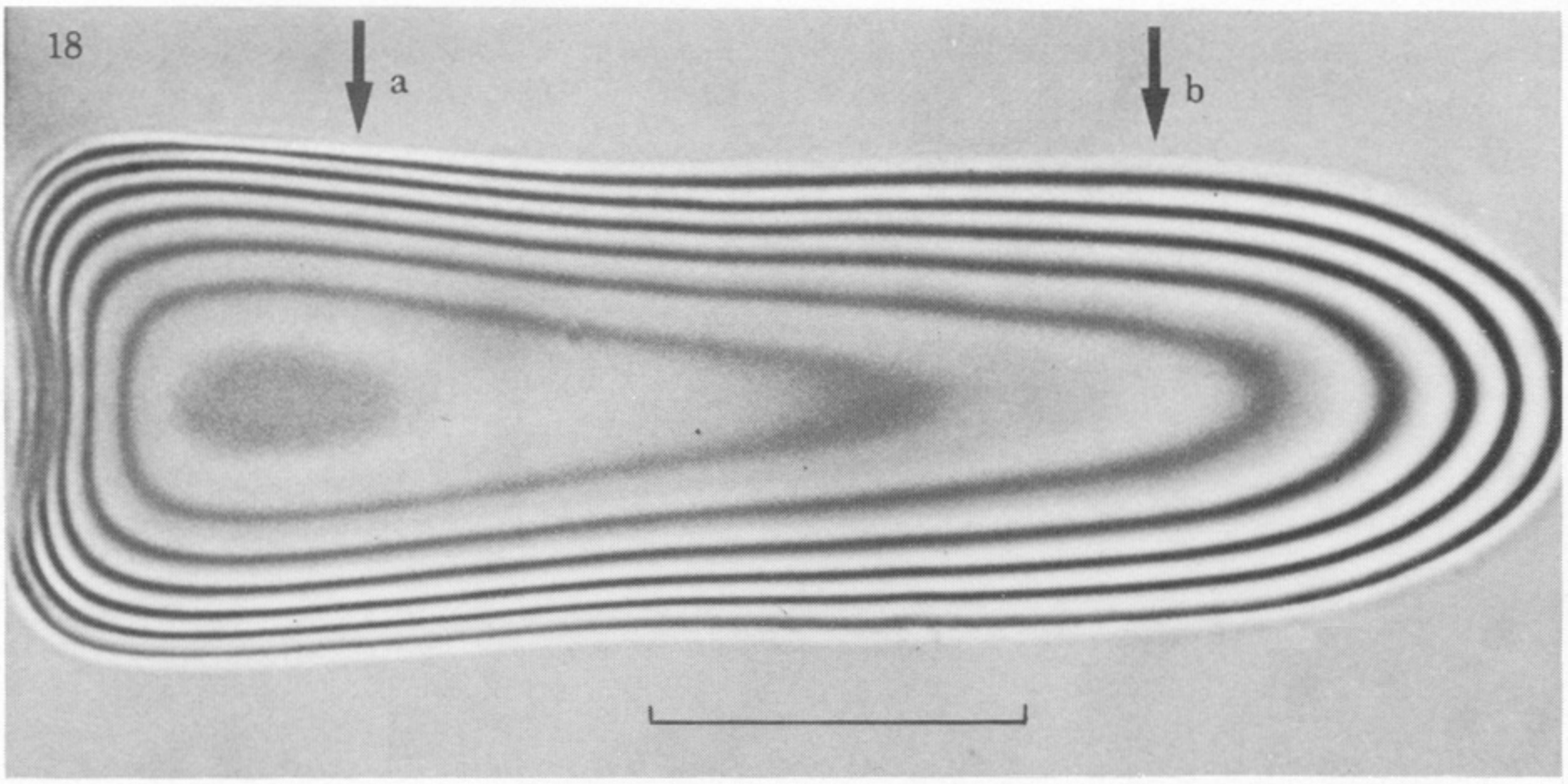

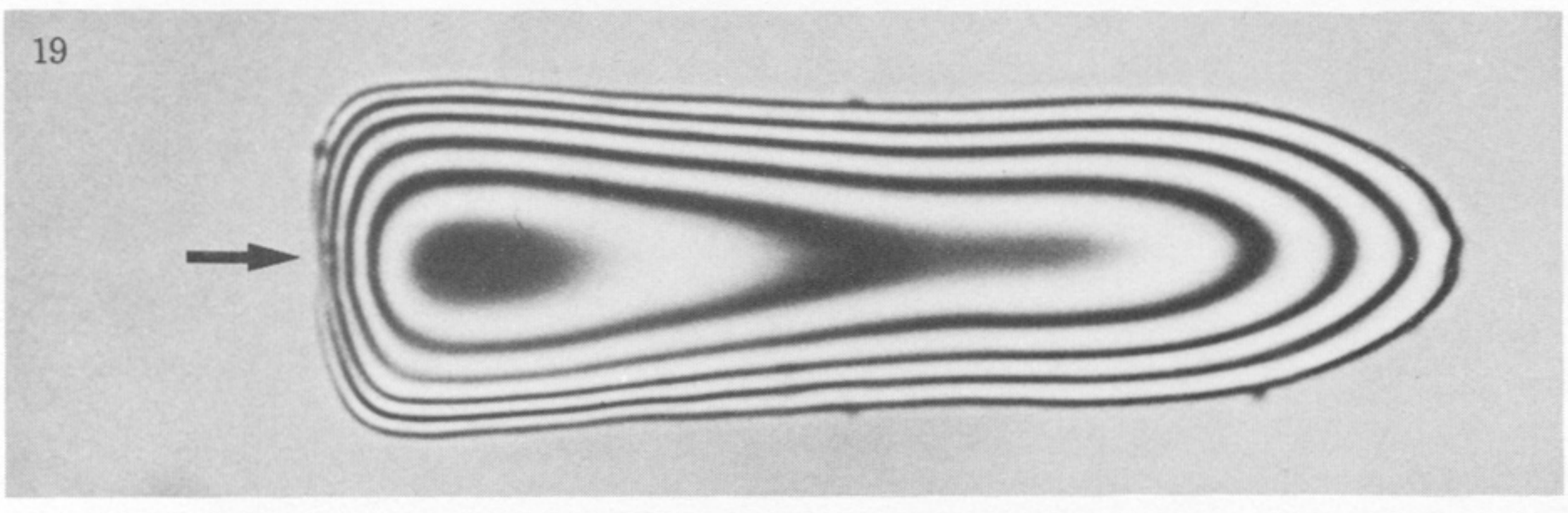

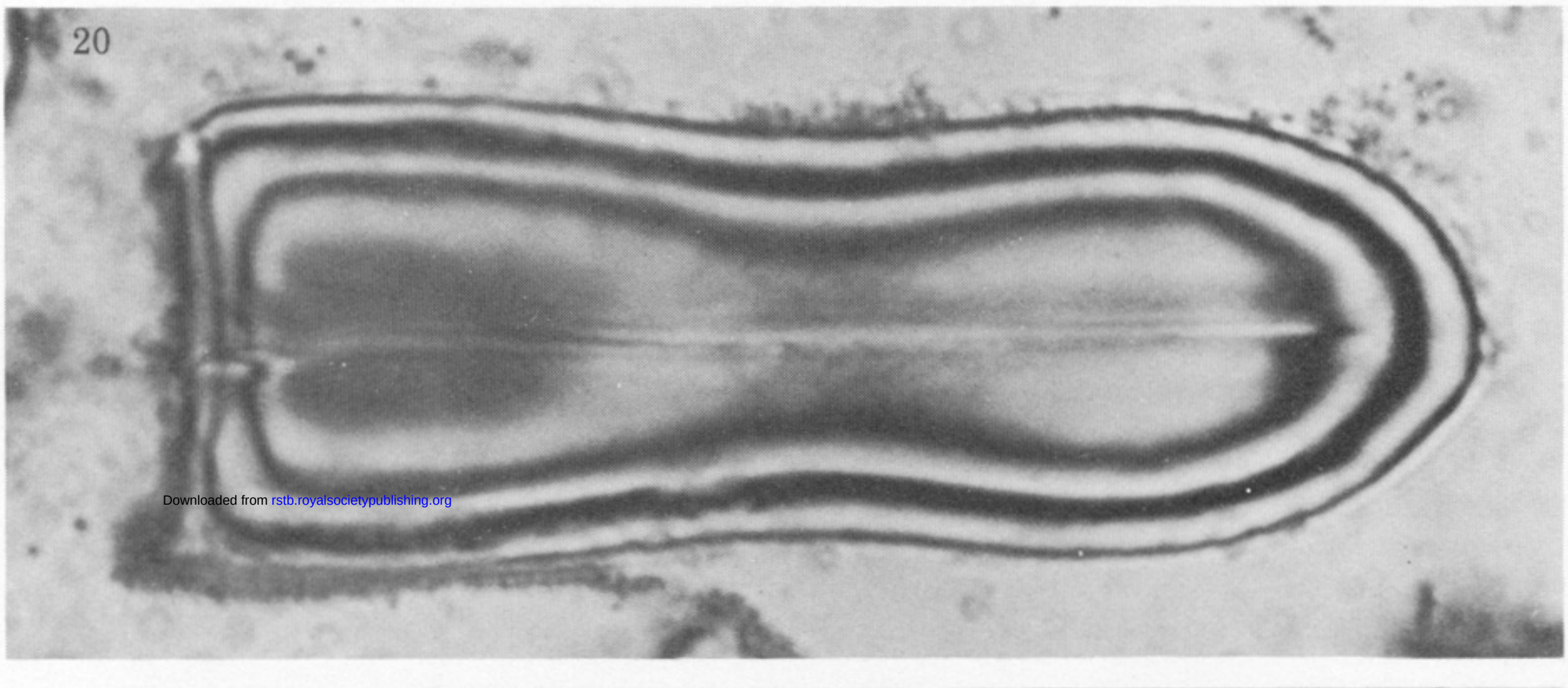

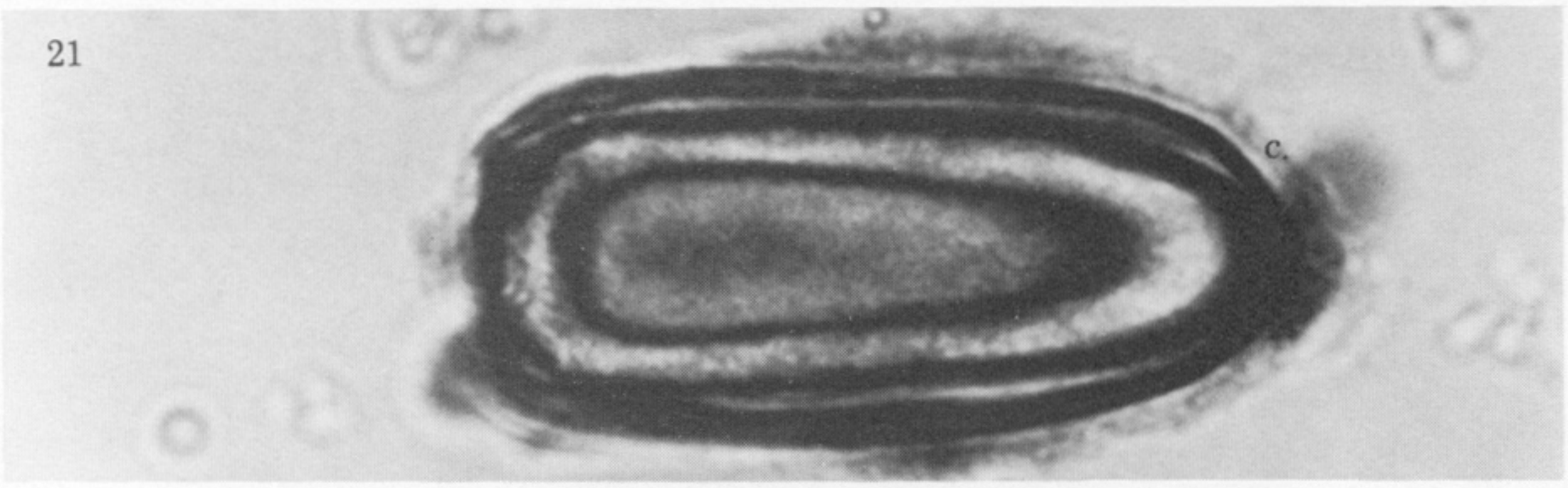

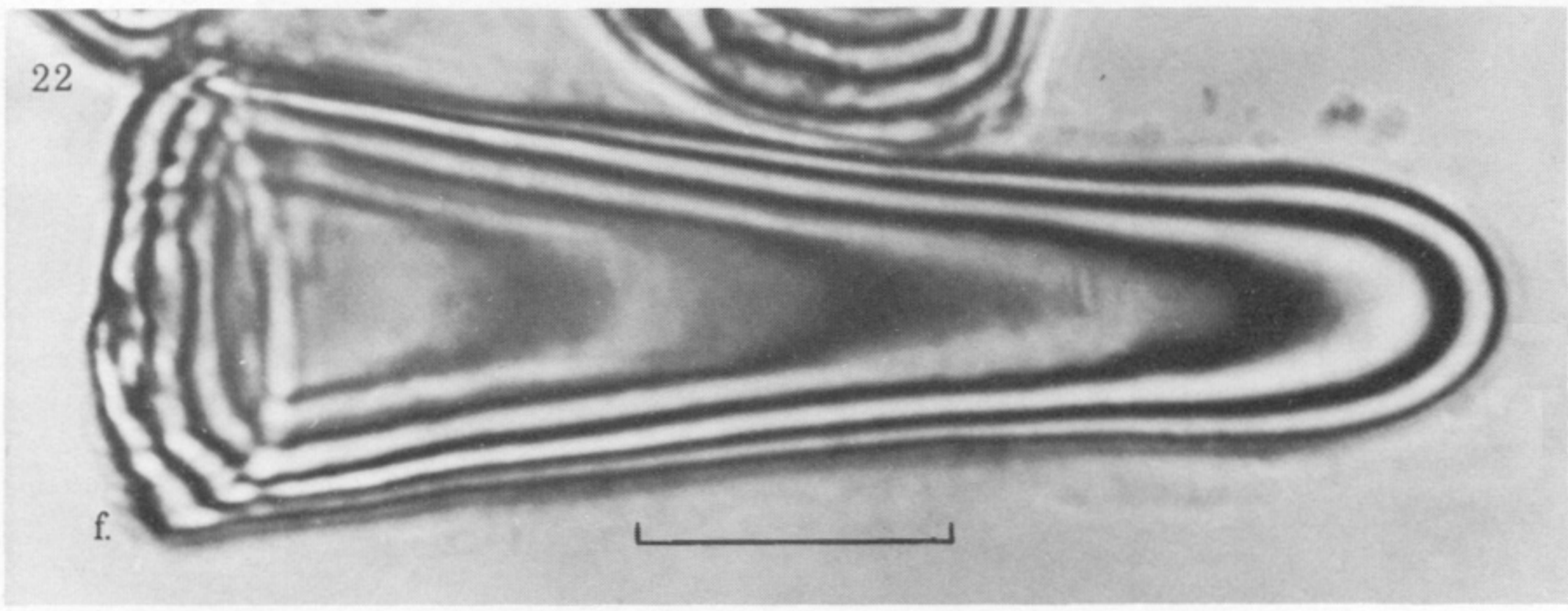

FIGURES 18–22. For description see opposite.